



Universiteit
Leiden
The Netherlands

PD-L1 checkpoint blockade promotes regulatory T cell activity that underlies therapy resistance

Gulijk, M. van; Krimpen, A. van; Schetters, S.; Eterman, M.; Elsas, M. van; Mankor, J.; ... ; Hall, T. van

Citation

Gulijk, M. van, Krimpen, A. van, Schetters, S., Eterman, M., Elsas, M. van, Mankor, J., ... Hall, T. van. (2023). PD-L1 checkpoint blockade promotes regulatory T cell activity that underlies therapy resistance. *Science Immunology*, 8(83). doi:10.1126/sciimmunol.abn6173

Version: Publisher's Version

License: [Licensed under Article 25fa Copyright Act/Law \(Amendment Taverne\)](#)

Downloaded from: <https://hdl.handle.net/1887/3768517>

Note: To cite this publication please use the final published version (if applicable).



IMMUNOTHERAPY

PD-L1 checkpoint blockade promotes regulatory T cell activity that underlies therapy resistance

Mandy van Gulijk^{1,2*}, Anneloes van Krimpen^{1,2,†}, Sjoerd Schetters^{3,†}, Mike Eterman^{1,2}, Marit van Elsas⁴, Joanne Mankor^{1,2}, Larissa Klaase¹, Marjolein de Bruijn¹, Menno van Nimwegen¹, Tim van Tienhoven¹, Wilfred van Ijcken⁵, Louis Boon⁶, Johan van der Schoot⁷, Martijn Verdoes^{7,8}, Ferenc Scheeren⁹, Sjoerd H. van der Burg⁴, Bart N. Lambrecht^{1,3,10}, Ralph Stadhouders^{1,11}, Floris Dammeijer^{1,2,*‡}, Joachim Aerts^{1,2,*‡}, Thorbald van Hall^{4,*‡}

Despite the clinical success of immune checkpoint blockade (ICB), in certain cancer types, most patients with cancer do not respond well. Furthermore, in patients for whom ICB is initially successful, this is often short-lived because of the development of resistance to ICB. The mechanisms underlying primary or secondary ICB resistance are incompletely understood. Here, we identified preferential activation and enhanced suppressive capacity of regulatory T cells (T_{reg} cells) in αPD-L1 therapy-resistant solid tumor-bearing mice. T_{reg} cell depletion reversed resistance to αPD-L1 with concomitant expansion of effector T cells. Moreover, we found that tumor-infiltrating T_{reg} cells in human patients with skin cancer, and in patients with non-small cell lung cancer, up-regulated a suppressive transcriptional gene program after ICB treatment, which correlated with lack of treatment response. αPD-1/PD-L1-induced PD-1⁺ T_{reg} cell activation was also seen in peripheral blood of patients with lung cancer and mesothelioma, especially in nonresponders. Together, these data reveal that treatment with αPD-1 and αPD-L1 unleashes the immunosuppressive role of T_{reg} cells, resulting in therapy resistance, suggesting that T_{reg} cell targeting is an important adjunct strategy to enhance therapeutic efficacy.

INTRODUCTION

Immune checkpoint blockade (ICB) using inhibitors to programmed cell death protein 1 or programmed death-ligand 1 (αPD-1/PD-L1) has revolutionized cancer therapy by unleashing T cell-mediated antitumor immunity, resulting in clinical responses in multiple cancer types, including melanoma and non-small cell lung cancer (NSCLC) (1). However, most patients with certain tumor types, including mesothelioma and small cell lung cancer (SCLC), do not experience durable clinical benefit from αPD-1/PD-L1 therapy for reasons largely unknown (2–4). Therefore, identification of the mechanisms responsible for therapy resistance remains essential to further boost efficacy of ICB therapy.

Regulatory T cells (T_{reg} cells) represent a major barrier to successful antitumor immunity because they are potent suppressors of effector T cells in the tumor microenvironment (TME) and lymphoid organs (5). Accordingly, the high abundance of T_{reg} cells relative to effector T cells in the TME is associated with poor

prognostic outcomes in multiple solid cancers (6, 7). In contrast, the absence of T_{reg} cells or genetic/pharmacological depletion of T_{reg} cells results in improved antitumor immunity and delayed tumor growth in multiple murine models (8–10). T_{reg} cells exert these immunosuppressive effects through multiple contact-dependent and soluble signaling mechanisms. These mechanisms include the scavenging of interleukin-2 (IL-2) through constitutive expression of the high affinity IL-2 receptor, containing the CD25 subunit; secretion of immunosuppressive molecules such as IL-10; and expression of inhibitory cell surface receptors like cytotoxic T-lymphocyte-associated protein 4 (CTLA-4) that impair effective costimulation of effector T cells by antigen-presenting cells (APCs) (5, 11, 12). Besides CTLA-4, T_{reg} cells express high levels of PD-1, but the functional consequence of αPD-1/PD-L1 therapy in this context remains incompletely understood (13–15). Recently, increased PD-1 expression in tumor-infiltrating T_{reg} cells compared with CD8⁺ T cells before αPD-1 treatment accurately predicted resistance to αPD-1/PD-L1 therapy and correlated with hyperprogressive disease (HPD) in patients with gastric cancer (16, 17). However, whether αPD-1/PD-L1 treatment-mediated activation of T_{reg} cells occurs beyond the rare phenomenon and is involved in therapy resistance remains largely unknown. Therefore, identifying the role and site of action of αPD-1/PD-L1 treatment on T_{reg} cells in the context of αPD-1/PD-L1 resistance could guide identification of targets aimed at rewiring T_{reg} cells and thus improve αPD-1/PD-L1 therapy efficacy.

In the present study, we found that αPD-L1 treatment preferentially activated T_{reg} cells in therapy-resistant tumor models but not effector T cells in both the TME and secondary lymphoid organs. αPD-L1 increased the suppressive capacity of T_{reg} cells, whereas T_{reg} cell depletion, in turn, sensitized both primary and secondary resistant tumor models to αPD-L1 treatment. Analysis of single-cell

¹Department of Pulmonary Medicine, Erasmus Medical Center Rotterdam, Rotterdam, Netherlands. ²Erasmus MC Cancer Institute, Erasmus Medical Center Rotterdam, Rotterdam, Netherlands. ³Laboratory of Immunoregulation and Mucosal Immunology, VIB-UGent Center for Inflammation Research, Ghent, Belgium. ⁴Department of Medical Oncology, Oncode Institute, Leiden University Medical Center, Leiden, Netherlands. ⁵Department of Biomics, Erasmus Medical Center Rotterdam, Rotterdam, Netherlands. ⁶JJP Biologics, Warsaw, Poland. ⁷Department of Tumor Immunology, Radboud Institute for Molecular Life Sciences, Radboud University Medical Center, Nijmegen, Netherlands. ⁸Institute for Chemical Immunology, Nijmegen, Netherlands. ⁹Department of Dermatology, Leiden University Medical Center, Leiden, Netherlands. ¹⁰Department of Internal Medicine and Pediatrics, Ghent University, Ghent, Belgium. ¹¹Department of Cell Biology, Erasmus Medical Center Rotterdam, Rotterdam, Netherlands.

*Corresponding author. Email: m.vangulijk@erasmusmc.nl (M.v.G.); f.dammeijer@erasmusmc.nl (F.D.); j.aerts@erasmusmc.nl (J.A.); t.van_hall@lumc.nl (T.v.H.)

†These authors contributed equally to this work.

‡These authors contributed equally to this work.

RNA sequencing (scRNA-seq) data of T_{reg} cells isolated from tumor biopsies before and after α PD-1 treatment revealed elevated expression of immune suppressive genes after α PD-1 treatment, specifically in nonresponding patients. PD-1⁺ T_{reg} cells in peripheral blood of patients with SCLC, NSCLC, and mesothelioma showed increased proliferation after α PD-1/PD-L1 treatment, specifically in nonresponding patients. These results indicate that T_{reg} cells are not mere bystanders but can be activated by α PD-1/PD-L1 treatment that associates with therapy resistance. This offers insights in the mechanisms underlying α PD-1/PD-L1 resistance and provides avenues for α PD-1/PD-L1 ICB biomarker and combination immunotherapy discovery.

RESULTS

α PD-L1 treatment induces preferential activation and proliferation of T_{reg} cells in therapy-resistant murine tumor models

To gain insight into the mechanisms responsible for ICB resistance, we studied the intraperitoneal AE17-OVA mesothelioma tumor model that is refractory to α PD-L1 therapy, because α PD-L1 treatment did not prolong survival, even when initiated early at day 5 (Fig. 1, A and B). T cell phenotype and activation status were measured in tumor-draining lymph nodes (mediastinal lymph node; TDLNs), non-TDLNs (inguinal LNs), spleen, blood, and tumor at several time points before and after α PD-L1 treatment (Fig. 1C). CD8⁺ T cells were only marginally activated after treatment in these tissues, with minor temporal up-regulation of costimulatory (e.g., 4-1BB, CD25, ICOS, and OX40) and coinhibitory markers (e.g., CD39, NKG2A, PD-1, LAG3, TIGIT, and CTLA-4) (Fig. 1D and figs. S1 and S2A). The same pattern was observed for the proliferation marker Ki67, which did not increase after α PD-L1 treatment in total CD8⁺ T cells or ovalbumin (OVA)-specific CD8⁺ T cells (fig. S2B). CD4⁺ T cells, however, displayed a more activated phenotype after treatment, including sustained expression of Ki67 and the exhaustion-program driver TOX. When discriminating between CD4-T helper (CD4-T_H) cells and T_{reg} cells on the basis of FoxP3 expression (fig. S2, C and D), the observed effect could largely be assigned to α PD-L1-induced activation of T_{reg} cells with induction of CTLA-4, Ki67, PD-1, and TOX 3 days after treatment (day 13). Proliferation was more profoundly induced in T_{reg} cells after α PD-L1 treatment compared with CD8⁺ T cells in the AE17-OVA model, whereas the opposite was observed in the α PD-L1-responsive MC38 tumor model (Fig. 1, E and F). Inclusion of a second therapy-responsive model (mesothelioma; AC29) and therapy-resistant model (melanoma; B16F10) showed the same pattern, with stronger induced proliferation in CD8⁺ T cells or T_{reg} cells in the responsive and resistant tumor models, respectively (Fig. 1G). Because checkpoint blockade may also affect immunity via myeloid cells, we examined alterations in these subsets after α PD-L1 treatment (18). α PD-L1 treatment appeared to have effects on myeloid cells that were less substantial compared with T_{reg} cells (fig. S3). Together, these results indicate that α PD-L1 could activate T_{reg} cells in the setting of primary therapy unresponsiveness.

α PD-L1 treatment amplifies the immunosuppressive phenotype and activity of T_{reg} cells

To comprehensively examine the effect of α PD-L1 treatment on T_{reg} cell phenotype, we investigated a wide variety of markers associated with the immunosuppressive function of T_{reg} cells in TDLN, non-TDLN, spleen, blood, and tumor material 3 days after α PD-L1 treatment. In the spleen, expression levels of key molecules associated with suppressive capacity of T_{reg} cells (ICOS, CTLA4, CD39, and PD-1) were significantly elevated in α PD-L1-treated mice compared with those given isotype treatment (Fig. 2A). This coincided with a tended increase in absolute T_{reg} cell numbers, whereas this was not observed for CD4-T_H cells or CD8⁺ T cells (fig. S4A). The pattern of enhanced expression of key suppressive molecules was also apparent in TDLNs, non-TDLNs, blood, and tumors, despite already higher basal expression levels on intratumoral T_{reg} cells (fig. S4B). We further assessed the effects of α PD-L1 treatment on tumor-derived T_{reg} cells in an unbiased manner by performing RNA sequencing. Pathway analysis of genes differentially expressed in α PD-L1-treated PD-1⁺ T_{reg} cells versus isotype-treated PD-1⁺ T_{reg} cells revealed enrichment for genes involved in T cell activation and apoptosis, whereas these pathways were not enriched in PD-1⁻ T_{reg} cells or CD4-T_H cells (Fig. 2B and fig. S5A). More specifically, α PD-L1-treated PD-1⁺ T_{reg} cells showed enhanced expression of key signature genes related to suppressive function such as *Il10*, *Tigit*, and *Icos* but also *Fgl2*, *Tsc1*, and *Ets1*, which were previously reported to mediate T_{reg} cell-suppressive activity (19–23) (Fig. 2C and fig. S5B). The up-regulation of genes related to suppressive function was less robust in PD-1⁻ T_{reg} cells and CD4-T_H cells, indicating a greater effect on the PD-1⁺ subpopulation (fig. S5C). In addition, α PD-L1 treatment induced a proapoptotic gene signature specifically in PD-1⁺ T_{reg} cells because antiapoptotic genes, including *Bcl2*, were down-regulated, whereas proapoptotic genes, such as *Bcl2l11* (encoding for BIM), were up-regulated (Fig. 2C and fig. S5B). The decreased *Bcl2*/BIM ratio was confirmed at the protein level and coincided with increased expression of activated caspase 3 (fig. S5D). Ki67 expression was higher in *Bcl2*⁻ T_{reg} cells compared with their *Bcl2*⁺ counterparts (fig. S5E). These data are in line with a recent report showing apoptotic T_{reg} cells to be superior in mediating immunosuppression compared with nonapoptotic T_{reg} cells (24). Therefore, these data indicate that T_{reg} cells, in particular PD-1⁺ T_{reg} cells, acquire a more immunosuppressive transcriptional signature after treatment.

Next, we examined whether α PD-L1-treated T_{reg} cells were also functionally more suppressive. To this end, we isolated T_{reg} cells from tumors and spleens by flow sorting from tumor-bearing FoxP3^{RFP} reporter mice treated with either isotype or α PD-L1. T_{reg} cells were subsequently cultured with naïve prelabeled responder CD8⁺ T cells in the presence of α CD3 monoclonal antibody and mitomycin-treated APCs (Fig. 2D and fig. S5F). Whereas CD8⁺ T cells proliferated vigorously in the absence of T_{reg} cells, this proliferation was reduced by addition of isotype-treated T_{reg} cells. α PD-L1 treatment resulted in tumor-derived T_{reg} cells with significantly more potent suppressive function than after isotype treatment (Fig. 2D). This α PD-L1-induced suppression was more marked in tumor-derived T_{reg} cells compared with spleen-derived T_{reg} cells (fig. S5F). Together, these data show that α PD-L1 treatment increases the suppressive capacity of T_{reg} cells in vivo.

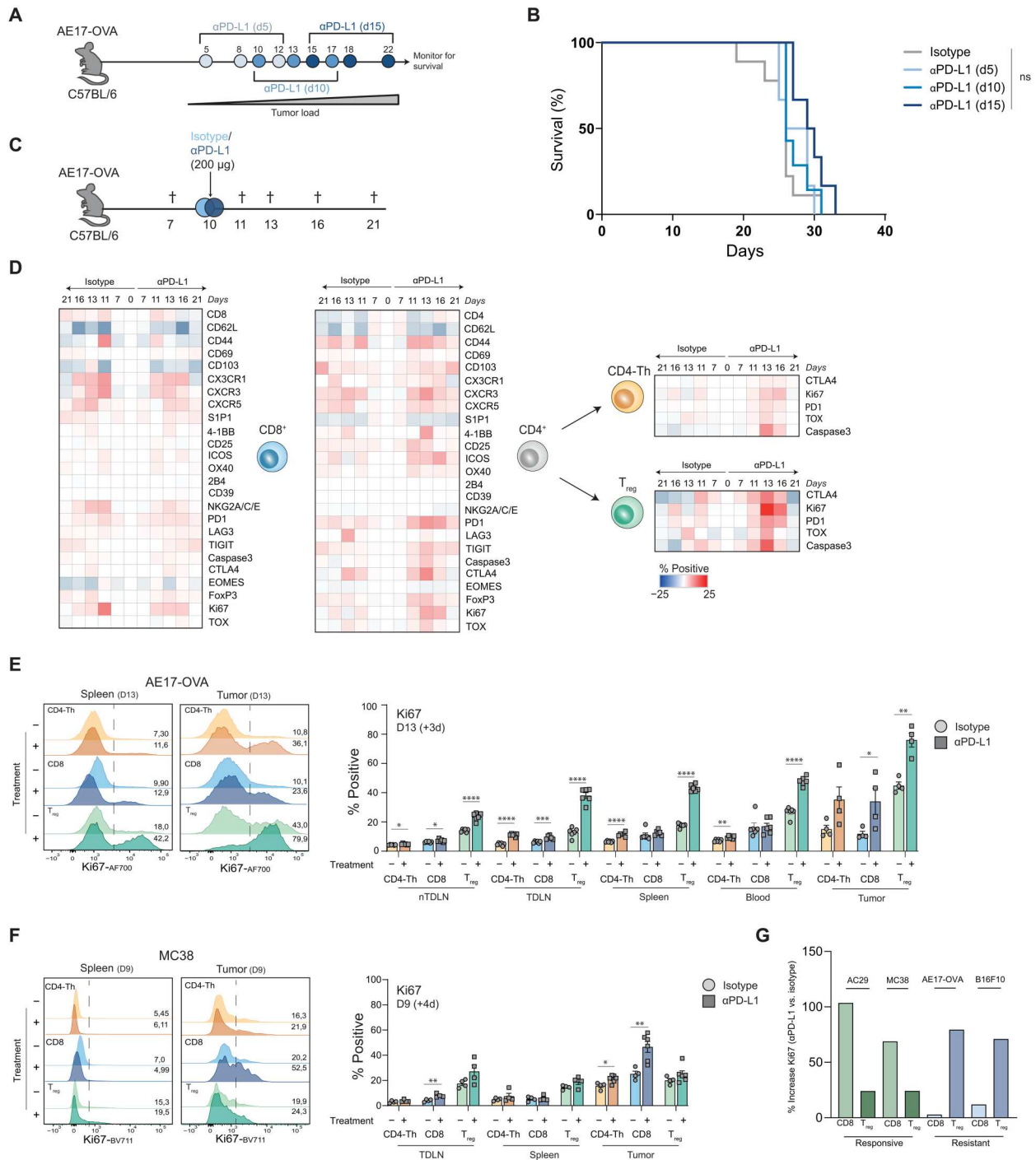


Fig. 1. αPD-L1 treatment specifically induces rapid activation of T_{reg} cells with marginal activation of CD8⁺ T cells and CD4-T_H cells in a therapy-resistant mesothelioma murine model. (A and B) Experimental setup (*n* = 3 to 7 mice per group) with mice being treated with systemic isotype or αPD-L1 antibodies intraperitoneally starting from day 5, 10, or 15 onwards and monitored for survival. Log rank tests were used to determine statistical significance. ns, not significant. (C) Experimental setup (*n* = 5 or 6 mice per group) with mice being treated with systemic isotype or αPD-L1 antibodies intraperitoneally at day 10 and euthanized at different time points before and after isotype and αPD-L1 treatment. (D) Protein expression of costimulatory, coinhibitory, and transcription factors were compared between isotype- and αPD-L1-treated mice at each indicated time point (days after tumor inoculation) by flow cytometry and displayed in heatmaps. Differences in percentage positive compared with day 0 (tumor-free mice) for each marker are displayed for spleen. (E and F) Representative histograms and quantification displaying Ki67 expression in spleen and tumor for CD4-T_H cells (orange), CD8⁺ T cells (blue), and T_{reg} cells (green) of isotype (–) and αPD-L1(+) treated AE17-OVA tumor-bearing mice (d13) (E) and MC38 tumor-bearing mice (d9) (F). (G) Bar graphs displaying differences in Ki67 expression in treated mice versus untreated mice for the AC29 mesothelioma (*n* = 7) and MC38 colon adenocarcinoma (*n* = 5 to 7; responsive models) and the AE17-OVA mesothelioma (*n* = 6) and B16F10 melanoma model (*n* = 8; resistant models) in peripheral blood at day 13, 3 days after treatment. Means and SEMs are shown, and unpaired *t* tests were performed, indicating statistical significance. **P* < 0.05, ****P* < 0.01, *****P* < 0.001, and ******P* < 0.0001.

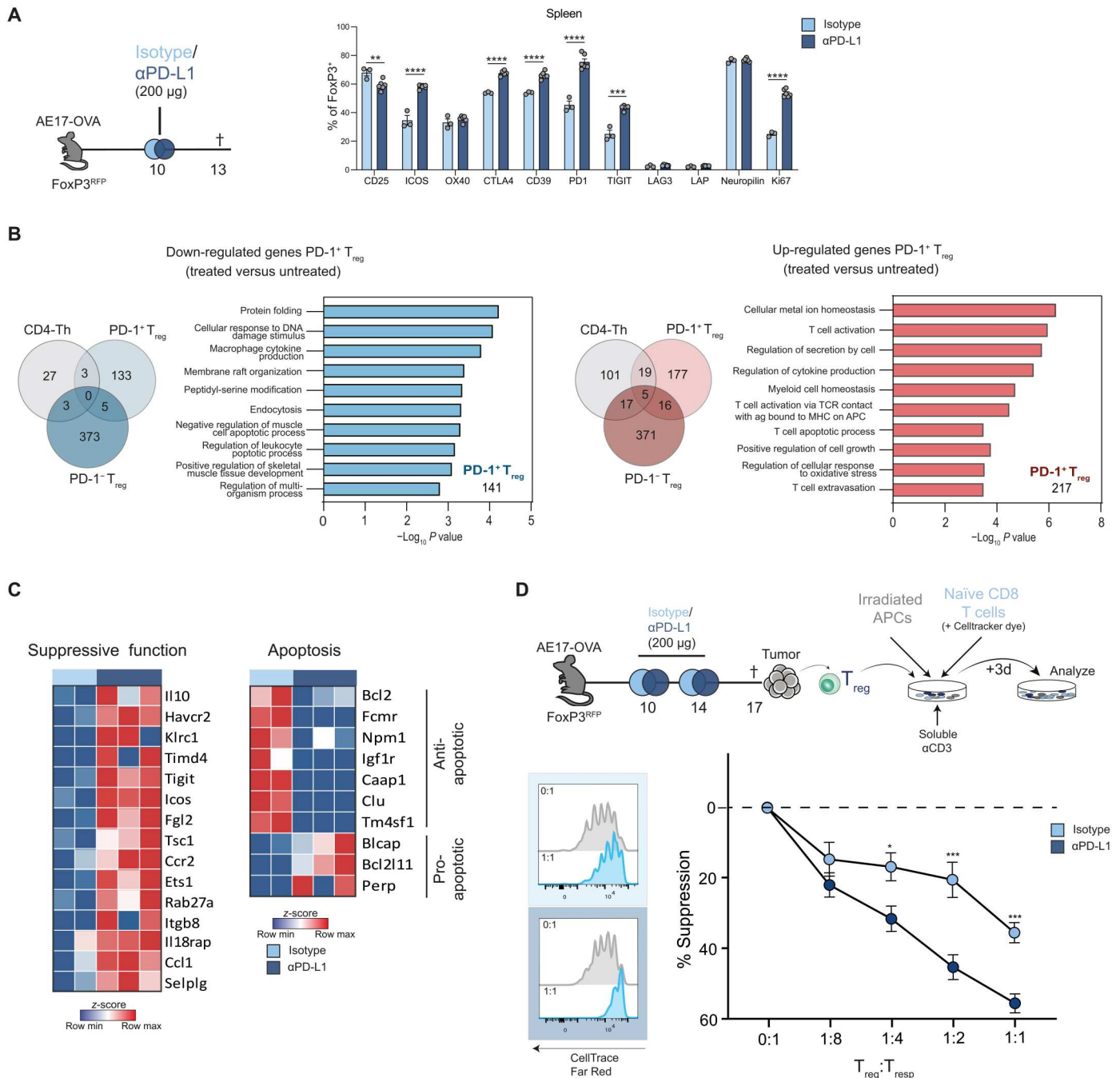


Fig. 2. αPD-L1 treatment enhances suppressive phenotype and capacity of T_{reg} cells. (A) Experimental setup ($n = 3$ to 6 mice per group) of AE17-OVA-bearing mice treated with isotype or αPD-L1 antibodies intraperitoneally at day 10 and euthanized at day 13 (left). Expression of markers associated with suppressive capacity of T_{reg} cells were assessed by flow cytometry and compared between isotype- and αPD-L1-treated mice in spleen (right). (B) Venn diagrams depicting overlap of genes (PD-1⁺ T_{reg} cells, PD-1⁻ T_{reg} cells, and CD4⁺ T_H cells) and pathway analysis (PD-1⁺ T_{reg} cells) of down-regulated (blue) or up-regulated (red) DEGs in αPD-L1 versus isotype treatment ($n = 2$ to 3 mice). Number in corners indicate the number of DEGs. (C) Heatmaps displaying DEGs in αPD-L1-treated versus isotype-treated PD-1⁺ T_{reg} cells (shown as z scores of RPKM levels with row min-max based on all three T cell subsets) associated with suppressive function and apoptosis. (D) Experimental setup of AE17-OVA-bearing FoxP3^{RFP} reporter mice treated with either isotype or αPD-L1 antibodies intraperitoneally at days 10 and 14 and euthanized at day 17. RFP⁺CD4⁺ T cells were sorted from tumors and cultured for 3 days with labeled naïve CD8⁺ T cells, mitomycin-irradiated T cell-depleted splenocytes (APCs), and soluble αCD3 for 3 days. Proliferation of naïve CD8⁺ T cells was assessed with different T_{reg}:T_{resp} ratios with T_{reg} cells from either isotype or αPD-L1-treated mice ($n = 8$ to 12) and depicted in histograms. Percent suppression was calculated as described in Materials and Methods. Means and SEMs are shown, and unpaired *t* tests were performed, indicating statistical significance. * $P < 0.05$, ** $P < 0.01$, *** $P < 0.001$, and **** $P < 0.0001$.

PD-1 exerts an important function in modulating T_{reg} cell phenotype after αPD-L1 treatment

To pinpoint whether the effect of αPD-L1 treatment is directly mediated via PD-1 expressed on T_{reg} cells, we performed a bone marrow chimera experiment, in which sublethally irradiated C57BL/6-CD45.1.2 recipient mice were reconstituted with a 1:1 mix of PD-1^{WT} CD45.1 and PD-1^{KO} CD45.2 donor bone marrow cells, allowing for donor reconstitution to be tracked and quantified using allele-specific CD45 antibodies. After reconstitution, recipient mice were inoculated with AE17-OVA tumor cells and treated with either isotype or αPD-L1 (Fig. 3, A and B). This setup allowed us to assess within the same animal whether αPD-L1 treatment enhanced T_{reg} cell proliferation by direct PD-1 uncoupling in T_{reg} cells or via T_{reg} cell-independent effects of αPD-L1 treatment. In accordance with our previous observations, basal levels of Ki67 expression were elevated in PD-1^{KO} T_{reg} cells as compared with PD-1^{WT} T_{reg} cells in isotype-treated animals (Fig. 3, B and C). αPD-L1 treatment significantly increased T_{reg} cell proliferation in PD-1^{WT} T_{reg} cells (up to 2- to 3-fold), and this appeared to be less in PD-1^{KO} T_{reg} cells (1- to 1.5-fold), pointing to an important cell-intrinsic role for PD-1 on T_{reg} cells in modulating T_{reg} cell phenotype.

Systemic depletion of T_{reg} cells reverts αPD-L1 resistance and improves immunotherapy efficacy

Although αPD-L1 treatment induced a more activated and immune suppressive phenotype of T_{reg} cells in the therapy-resistant AE17-OVA murine tumor model, it remained unclear whether this actively promoted therapy resistance. To this end, we treated FoxP3^{DTR} mice with diphtheria toxin (DT) to deplete T_{reg} cells, followed by

isotype or αPD-L1 treatment (Fig. 4A). DT treatment alone resulted in decreased tumor burden. When T_{reg} cell depletion was combined with αPD-L1 treatment, tumor burden was further reduced to near absence that was accompanied by an overt increase in memory tumor-infiltrating lymphocytes (TILs), demonstrating that T_{reg} cells are involved in therapy resistance (Fig. 4B). As a more translational approach, we then systemically depleted T_{reg} cells using an Fc-optimized αCD25 antibody in the therapy-resistant AE17-OVA tumor model (8, 25) (Fig. 4C). First, we could confirm that αCD25 treatment effectively decreased T_{reg} cells at multiple sites including secondary lymphoid organs and especially tumors rapidly after treatment, resulting in enhanced CD8⁺ T cell/T_{reg} cell ratios (Fig. 4D and fig. S6, A and B). Second, αCD25 treatment before αPD-L1 treatment led to a synergistic induction of CD8⁺ and CD4-T_H cell proliferation and activation in peripheral blood after immunotherapy, which was also observed in the therapy-resistant B16F10 tumor model (Fig. 4, E to G, and fig. S6C). Last, T_{reg} cell depletion sensitized AE17-OVA tumors for αPD-L1 treatment as observed by prolonged survival and decreased tumor weight (day 17), although all mice eventually succumbed because of progressive tumor growth (Fig. 4H). A similar effect was induced in the B16F10 model, with half of the mice showing prolonged survival and delayed tumor growth (Fig. 4I and fig. S6D). Although MC38-bearing mice were initially responsive to αPD-L1 treatment with reduced tumor growth (Fig. 4J, inset), mice eventually relapsed because of acquired resistance and did not show prolonged survival. Combination treatment, however, induced long-term survival in most of the mice (Fig. 4J). Whether αPD-L1 treatment exacerbates T_{reg} cell induced immunosuppression in this model as compared

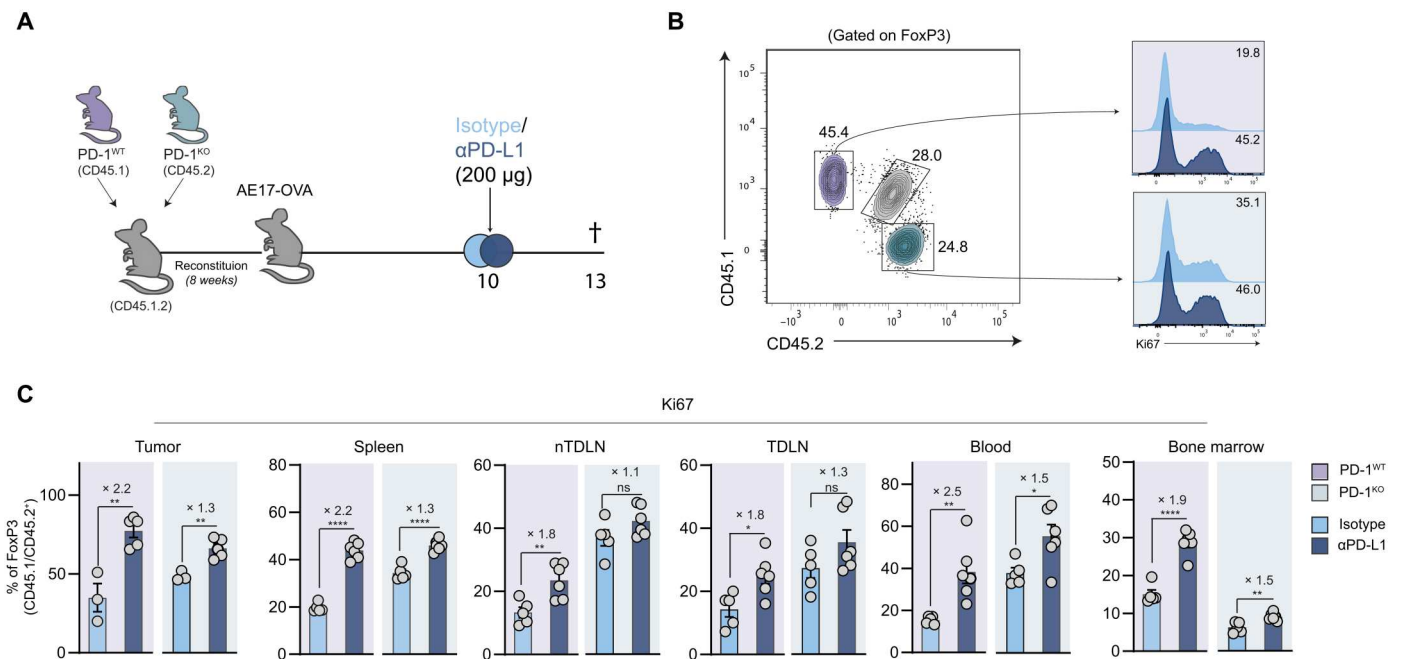
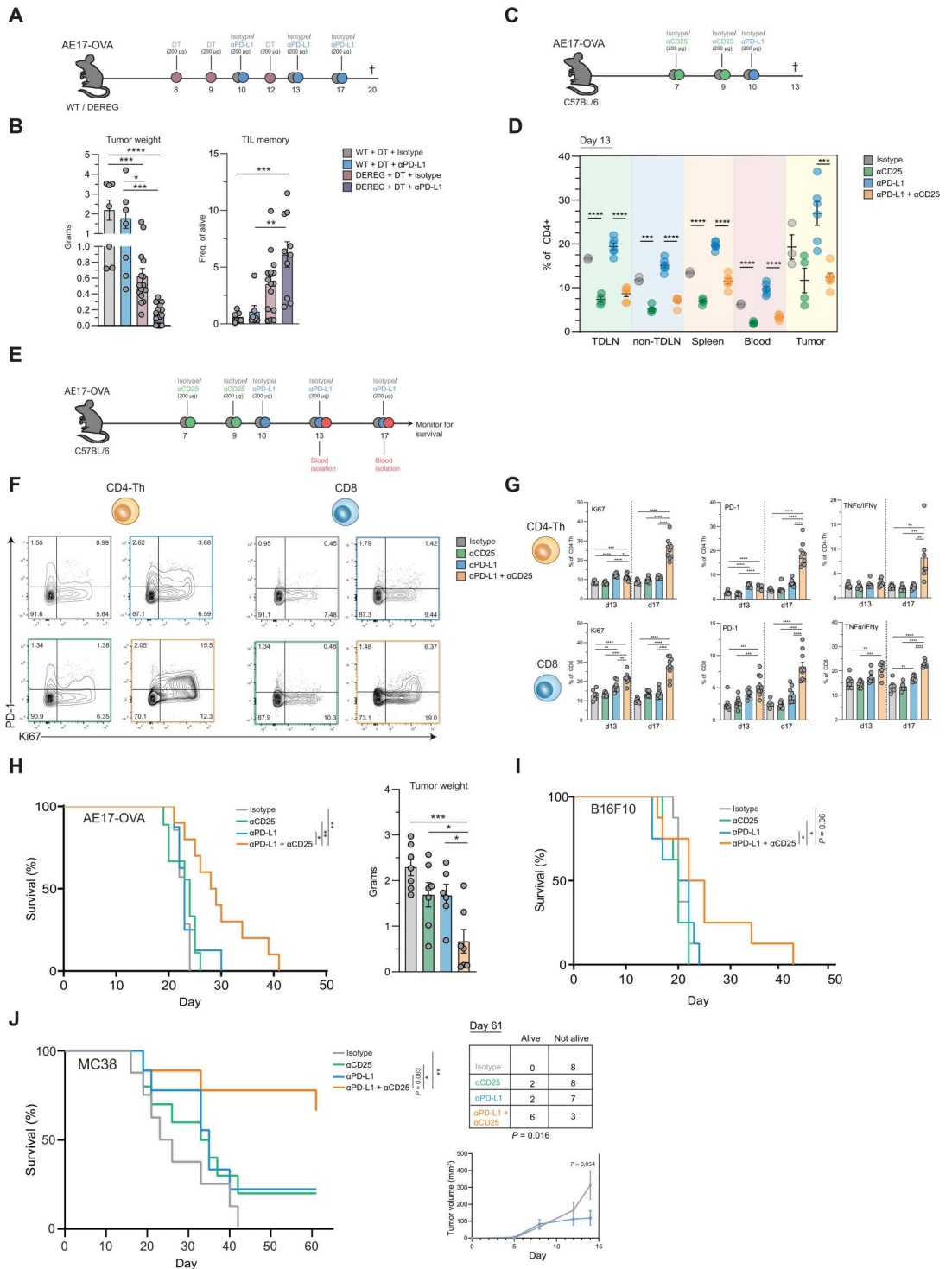


Fig. 3. PD-1 exerts an important function in mediating αPD-L1-induced effects on T_{reg} cells. (A) Experimental design with sublethally irradiated CD45.1.2 recipient mice being reconstituted with CD45.1 PD-1^{WT} and (purple) CD45.2 PD-1^{KO} (green) bone marrow cells followed by AE17-OVA inoculation and treatment with either isotype ($n = 5$) or αPD-L1 ($n = 6$). Mice were euthanized at day 13, and proliferation of PD-1^{WT} and PD-1^{KO} T_{reg} cells was evaluated in multiple tissues. (B) Proportions of CD45.1/CD45.2 T_{reg} cell populations and their level of proliferation, as depicted in histograms of intracellular Ki67 levels, at day 13 in spleen (3 days after treatment). (C) Percentage of T_{reg} cells (PD-1^{WT} and PD-1^{KO}) positive for Ki67 after isotype or αPD-L1 treatment in multiple tissues at day 13. Means and SEMs are shown, and unpaired t tests were performed, indicating statistical significance. * $P < 0.05$, ** $P < 0.01$, *** $P < 0.001$, and **** $P < 0.0001$.

Fig. 4. α PD-L1 therapy resistance is reverted by T_{reg} cell depletion by improving antitumor immunity and survival. (A) Experimental design where wild-type or DERE mice ($n = 7$ to 16 mice per group) were treated with DT followed by either isotype or α PD-L1 treatment at days 10, 13, and 17. Mice were euthanized at day 20. (B) Bar graphs displaying tumor weights (left) and the percentage of memory $CD8^+$ T cells infiltrating the tumor (right) for the different treatment groups at day 17. (C) Experimental design during which mice bearing AE17-OVA tumors ($n = 8$ to 10 per group) were treated with isotype or α CD25 mIgG2a T_{reg} cell-depleting antibody at days 7 and 9 followed by α PD-L1 treatment at day 10. (D) Mice were euthanized at day 13 to assess T_{reg} cell frequencies in TDLNs, non-TDLNs, spleen, blood, and tumors. (E) Immunotherapeutic protocol of α PD-L1 treatment at days 10, 13, and 17 in the presence of T_{reg} cell-depleting antibody at days 7 and 9. Peripheral blood was isolated from the tail vein at days 13 and 17, and mice were monitored for survival. (F) Representative flow cytometry plots displaying level of proliferation (Ki67) for different treatment groups in $CD4^+$ T_H cells and $CD8^+$ T cells in peripheral blood at day 17. (G) Quantification of level of proliferation (Ki67), PD-1 expression, and expression of $TNF\alpha$ and $IFN\gamma$ at days 13 and 17 for both $CD4^+$ T_H cells and $CD8^+$ T cells in peripheral blood. (H) Kaplan-Meier curves of the experiment in E showing tumor survival and bar graphs displaying tumor weights at day 17 ($n = 7$ per group). (I) Kaplan-Meier curves of checkpoint-resistant B16F10-bearing mice treated with the same protocol as AE17-OVA-bearing mice in (E). (J) Kaplan-Meier curves of checkpoint-sensitive MC38-bearing mice treated with α CD25 mIgG2a at days 5 and 7 and α PD-L1 treatment at days 5, 8, and 11 ($n = 8$ to 10 per group). Log rank tests were used to determine statistical significance. Chi-square test was performed to assess the association of treatment and survival at day 61. Tumors were measured for 14 days after inoculation in mice treated with isotype and α PD-L1. Means and SEMs are shown, and for comparisons between two groups, unpaired t test was used. For comparisons between multiple groups, one-way (G and H) or two-way (B) ANOVA was used with multiple-comparison tests. * $P < 0.05$, ** $P < 0.01$, *** $P < 0.001$, and **** $P < 0.0001$.



Downloaded from <https://www.science.org> at Leiden University on July 16, 2024

with the primary resistant models remains to be investigated. These data show that T_{reg} cells are involved in both primary and secondary therapy resistance to α PD-L1 treatment in preclinical solid mouse tumor models.

T_{reg} cell activation in patient tumor biopsies and peripheral blood after ICB treatment is associated with poor treatment response

Although we observed robust treatment-induced augmentation of T_{reg} cell effector functions in preclinical murine models, effects of α PD-1/PD-L1 treatment on T_{reg} cells in a clinical setting and its association with treatment response remain unclear. We therefore assessed the effects of α PD-1 treatment on tumor-infiltrating T_{reg} cells in publicly available scRNA-seq data from site-matched tumor biopsies of responding and nonresponding patients with nonmelanoma skin cancer (BCC) or NSCLC before and after α PD-1 treatment (Fig. 5A) (26, 27). Phenotypically similar T_{reg} cells were extracted from these datasets, and gene expression was compared before treatment and after treatment in both responders and nonresponders (table S1 and fig. S7, A and B). Nonresponding patients with BCC and NSCLC shared 64 up-regulated genes in T_{reg} cells after treatment as compared with before treatment, including *PDCD1* encoding PD-1, whereas little to no overlap was seen for responding patients after treatment or in pretreatment comparisons (Fig. 5B and fig. S7, C to F). Pathway enrichment analysis of the differentially expressed genes (DEGs) up-regulated after treatment revealed genes significantly associated with (the regulation of) cell activation and apoptosis, specifically in nonresponding patients with BCC and NSCLC (Fig. 5C). In agreement, a gene set enrichment analysis (GSEA) showed significant enrichment of genes involved in the "Negative regulation of α/β T-cell activation" pathway among genes up-regulated after treatment only in nonresponders (Fig. 5, C and D). When comparing T_{reg} cell transcriptomes after treatment between responding and nonresponding patients with BCC and NSCLC, we observed a shared signature of treatment-induced genes involved in cell activation and enhanced suppressive capacity of T_{reg} cells (Fig. 5, E to H). These included genes related to T_{reg} cell-mediated suppression (e.g., *PDCD1*, *CTLA4*, *HAVCR2*, and *CD38*), T cell receptor signaling (e.g., *JUN/FOS* and *LAT*), and the cell cycle (*MKI67*), which were expressed at higher average levels and at greater frequencies in T_{reg} cells from nonresponders (Fig. 5, H and I). Only a few genes were up-regulated in responders after treatment, showing no overlap between both tumor types and no functional links with T_{reg} cell activation or suppressive capacity (fig. S7, G and H). Together, these data suggest that α PD-1 treatment induces an immunosuppressive activation program specifically in T_{reg} cells from nonresponding patients.

To assess whether differences in the T_{reg} cell phenotype at baseline could be linked to therapy resistance, we compared nonresponding and responding patients before treatment for both tumor types. BCC and NSCLC T_{reg} cells showed fewer overlapping gene expression signatures before treatment as compared with after treatment (80 DEGs versus 776 DEGs, respectively; see Fig. 5E and fig. S8, A to D), suggesting that shared therapy resistance mechanisms could be acquired during treatment or are more tumor specific at baseline. Pathway enrichment analysis of the (largely unique) pretreatment DEGs from both tumor types did indicate a more activated T_{reg} cell phenotype specifically in nonresponding patients with BCC and NSCLC (fig. S8B). These data suggest that T_{reg} cells are

already more activated at baseline in patients who subsequently experience therapy resistance after α PD-1 treatment.

To further explore whether ICB-induced T_{reg} cell activation and proliferation is related to clinical therapy efficacy, we characterized T_{reg} cells in paired pre- and posttreatment peripheral blood samples of three independent cohorts: α PD-L1-resistant patients with stage IV SCLC, patients with mesothelioma, and patients with stage IV NSCLC (table S2). Advanced SCLC tumors bear among the highest tumor mutational burdens but are considered largely refractory to α PD-(L)1 monotherapy, with only limited additional benefit when combined with first-line combination chemotherapy (28, 29). For all three tumor types, we observed a greater increase in proliferation after α PD-1/PD-L1-containing treatment in PD-1⁺ T_{reg} cells but not in PD-1⁻ T_{reg} cells, suggesting a direct effect of treatment via PD-1 on T_{reg} cells (Fig. 6A). Because we could dissect responding (R), including complete responses and partial responses, and nonresponding patients (NR) for NSCLC and mesothelioma, we examined whether the impact of α PD-1/PD-L1 treatment in PD-1⁺ T_{reg} cells correlated with response to treatment in these patient cohorts. We detected significantly enhanced levels of proliferation after treatment in PD-1⁺ T_{reg} cells but not in PD-1⁻ T_{reg} cells in nonresponding patients with NSCLC and mesothelioma (Fig. 6, B and C and fig. S9, A and B). This effect appeared to be enriched in nonresponding patients because PD-1⁺ T_{reg} cells proliferated less robustly in patients with clinical response to α PD-1/PD-L1 treatment. No clear correlations with response were found in the PD-1⁺ and PD-1⁻ effector CD4⁺ and CD8⁺ T cell populations (fig. S9, C to H). These data indicate that α PD-1/PD-L1 treatment affects PD-1⁺ T_{reg} cell proliferation in patients with cancer and that this associates with resistance to α PD-1/PD-L1 therapy.

DISCUSSION

In this study, we show that T_{reg} cells are not just exerting their known immunosuppressive role in cancer as a default characteristic but that this suppression is itself regulated by cell-intrinsic PD-1 engagement. Clinical use of α PD-1/PD-L1 unleashes this form of regulation, leading to enhanced T_{reg} cell immunosuppression and underlying therapy resistance. The data underline the importance of rational combination immunotherapy designs to specifically induce effector antitumor T cell populations without concomitant immune suppression through ICB-activated T_{reg} cells.

Recently, Kamada *et al.* reported that increased T_{reg} cell activity after α PD-1 treatment in patients with gastric cancer was associated with HPD (17). In addition, Kumagai *et al.* demonstrated that the balance of PD-1 expression on CD8⁺ T cells and T_{reg} cells before treatment in the TME predicted immunotherapy efficacy in NSCLC and gastric cancer. We elaborated on these findings, showing that the undesirable effect of α PD-1/PD-L1 treatment on T_{reg} cells could be more widespread, as evidenced by a significant subset of nonresponding patients showing increased T_{reg} cell proliferation after α PD-1/PD-L1 treatment. A small subset of responding patients displayed increased PD-1⁺ T_{reg} cell proliferation, not necessarily in parallel with increased effector T cell proliferation, suggesting that alternative mechanisms underlying α PD-1/PD-L1 response are at play, as documented by others (30).

In addition to enhanced expression of genes related to immunosuppression by T_{reg} cells after treatment, we show that T_{reg} cells also acquire a more proapoptotic gene expression program. These data

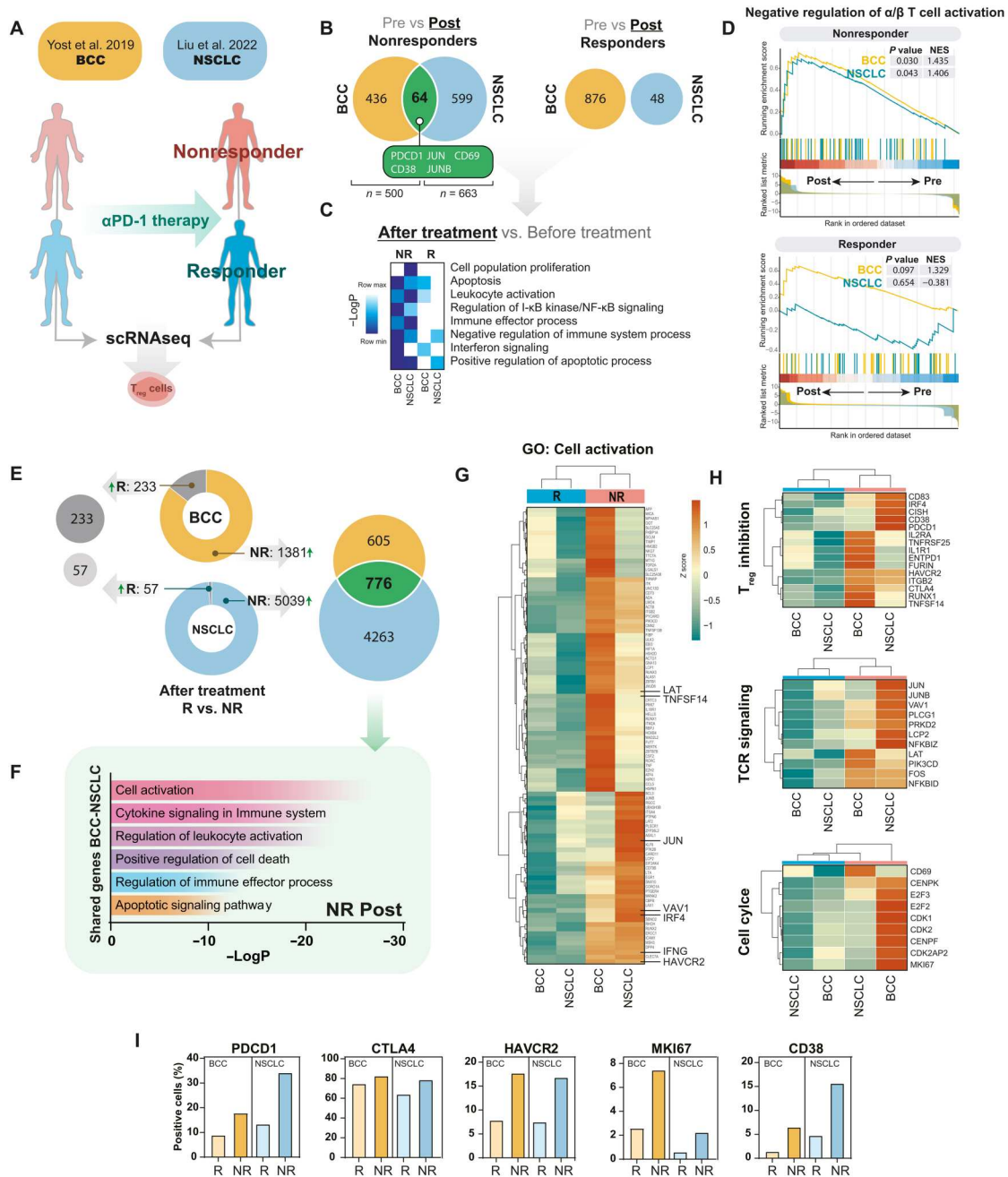


Fig. 5. T_{reg} cells in the TME of αPD-1-resistant patients with cancer up-regulate a transcriptional program linked to enhanced immunosuppression after treatment. (A) Predefined T_{reg} cell clusters were isolated from published BCC and NSCLC tumor scRNA-seq datasets in which biopsies were taken before (pre) and after (post) treatment with anti-PD-1 therapy (pembrolizumab). Patients were classified as either responders or nonresponders on the basis of RECIST v1.1. (B) Venn diagrams displaying overlap in genes up-regulated after treatment (as compared with pretreatment samples) from comparisons of T_{reg} cells in either nonresponder (left) or responder (right) patients with BCC and NSCLC. Genes of interest in the overlap are highlighted. (C) Pathway enrichment analysis displaying overlap in biological pathways associated ($P < 0.05$) with significantly up-regulated genes after versus before treatment in BCC and NSCLC T_{reg} cells [input genes are shown in (B), separated by therapy response (NR = nonresponder, R = responder)]. Strength of association is visualized by a Z-score of the $-\log_{10}$ -transformed P values. (D) GSEA plots (including genes with an absolute \log_2 fold change > 0.5) comparing T_{reg} cell transcriptomes before versus after treatment of nonresponders (top) and responders (bottom) from BCC and NSCLC for the “Negative regulation of alpha/beta T-cell activation” pathway (GO:0046636). (E) Donut plot of up- and down-regulated genes comparing responder with nonresponder patients after treatment. The arrows indicate the number of up-regulated genes per indicated patient group. Venn diagrams display the overlap in up-regulated genes between the BCC and NSCLC datasets of responders and nonresponders. (F) Pathway enrichment analysis of genes up-regulated in nonresponders compared with responders after treatment that are shared between the BCC and NSCLC datasets. The association strength of pathways is displayed by $-\log_{10}$ -transformed P values. (G) Hierarchically clustered heatmap displaying scaled expression levels of genes included in the “Cell activation” pathway (GO:0001775). (H) Hierarchically clustered heatmaps showing scaled expression levels for selected genes relevant for the indicated biological functions. (I) Percentage of positive cells (i.e., displaying a transcript count > 0) for selected genes. (B and C and E to I) Adjusted P value (FDR) < 0.05 and absolute \log_2 fold change > 0.5 . BCC, basal cell carcinoma.

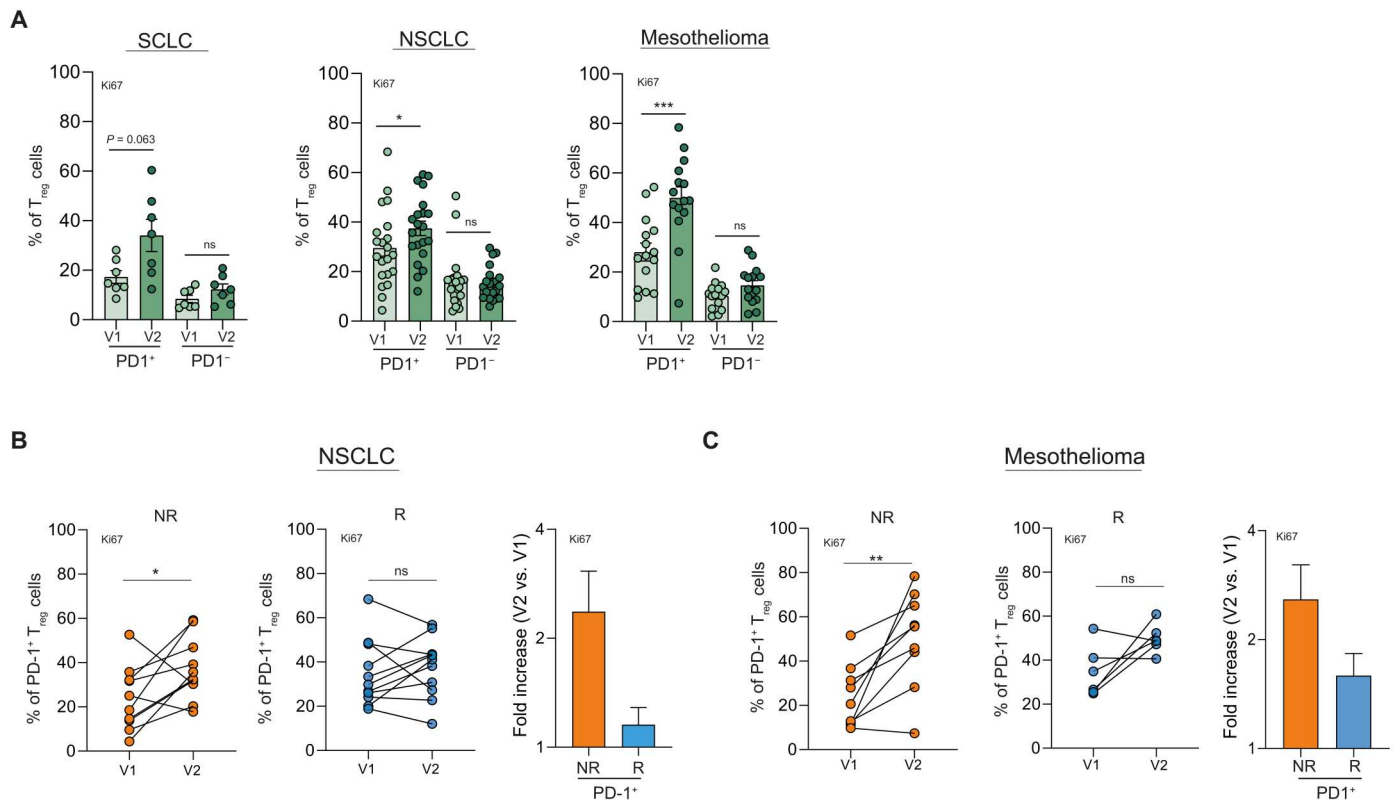


Fig. 6. Increased proliferation of PD-1⁺ T_{reg} cells in peripheral blood after αPD-1/αPD-L1 treatment is associated with therapy resistance. (A) Level of proliferation (Ki67) was assessed in PD-1⁺ and PD-1⁻ T_{reg} cells at baseline (V1) and 2 weeks after the start of αPD-1/PD-L1 treatment (V2) in peripheral blood of patients with SCLC, NSCLC, and mesothelioma. Increased proliferation after treatment start was determined in PD-1⁺ and PD-1⁻ T_{reg} cells and expressed as fold change in nonresponding (NR) and responding (R) patients with NSCLC (**B**) and patients with mesothelioma (**C**). Means and SEMs are shown, and paired t tests were performed, indicating statistical significance. **P* < 0.05, ***P* < 0.01, ****P* < 0.001, and *****P* < 0.0001.

confirm earlier findings in a graft-versus-host disease model demonstrating superior immunosuppressive activity after PD-1 blockade by apoptotic T_{reg} cells compared with their nonapoptotic counterparts (24). Apoptotic T_{reg} cells abolished αPD-L1 efficacy in various tumor models (24, 31). However, data obtained in claudin-low murine breast cancer, commonly linked to triple-negative breast cancer, suggest that αPD-1 treatment can promote the survival of T_{reg} cells (32). Factors such as timing, tumor model, and antibody used could account for this discrepancy. Future efforts should confirm whether, upon excess stimulation, T_{reg} cells benefit from an apoptotic phenotype and whether reverting T_{reg} cell apoptosis could improve the efficacy of αPD-1/PD-L1 therapy.

Our data indicate that PD-1 exerts an important function in directly modulating T_{reg} cell phenotype after αPD-L1 treatment. These findings align with recent data showing PD-1-deficient T_{reg} cells to be superior immunosuppressors compared with their wild-type counterparts (17, 33–35). The direct effect mitigated via PD-1 expressed on T_{reg} cells appeared not to be exclusive, and it is tempting to speculate that besides direct effects, indirect effects mediated via mechanisms such as the modulation of APCs are also at play. Future research in αPD-1/PD-L1-resistant tumor-bearing mice and in models with a T_{reg} cell-specific PD-1 deficiency could shed further light on this hypothesis. However, because genetic deletion of PD-1 on T_{reg} cells will likely mimic αPD-1/PD-L1

antibody-mediated T_{reg} cell activation, therapeutic efficacy may already be compromised.

How PD-1 blockade could affect downstream receptor signaling in T_{reg} cells remains incompletely understood. In line with its impact on effector T cells, PD-1 signaling in T_{reg} cells decreased phosphatidylinositol 3-kinase (PI3K)–AKT signaling, whereas antibody-mediated blockade or genetic ablation enhanced suppressive capacity in a murine tumor model (16). These data are in sharp contrast with data derived from an autoimmune encephalomyelitis model where PD-1 deficiency in T_{reg} cells resulted in diminished PI3K–AKT signaling, whereas an AKT activator reduced suppressive activity (34). These contrasting effects of PD-1 signaling in T_{reg} cells may be explained by different disease settings or specific rewiring of T_{reg} cells depending on the metabolic milieu. For example, lactic acid in the TME is important for T_{reg} cell immune suppressive function and the resultant efficacy of αCTLA4 therapy (36–39). Therefore, context-specific adjustments in T_{reg} cells may profoundly influence the net effect of PD-1 signaling on T_{reg} cells.

Our temporal analysis across multiple organs indicates that αPD-1/PD-L1-mediated effects on T_{reg} cells are systemically mediated. Others have previously indicated the importance of peripheral lymphoid tissues in generating effective αPD-1/PD-L1 efficacy, and we have recently demonstrated a critical role for TDLNs in generating progenitor exhausted T cells after ICB that subsequently seed the tumor (40–42). T_{reg} cells in the TDLN have already been shown

to mediate a role in antitumor immunity by restraining tumor invasion in patients with breast cancer, whereas T_{reg} cells in tumors were dysfunctional (43). In the context of α PD-1/PD-L1 resistance, durable therapy resistance may therefore not only depend on α PD-1/PD-L1-mediated activation of T_{reg} cells in the TME but also on activation of T_{reg} cells in peripheral lymphoid tissues, including the TDLN, that are recruited to the tumor. Selective PD-L1 blockade or T_{reg} cell depletion in TDLNs could provide clues to the location and mechanisms of T_{reg} cell-mediated T cell suppression.

To date, clinical efficacy of manipulation of T_{reg} cell number or function by CD25-directed antibodies is restricted. Development of novel CD25-depleting antibodies that preserves CD25 signaling in the effector T cell compartment offers opportunities (44). In addition, the discovery and clinical investigation of targets increased by checkpoint blockade, such as TIGIT, or recently identified T_{reg} cell targets, including endoglin, MCT1, and BATF, could offer avenues in attenuating ICB-mediated T_{reg} cell activation (45–47). However, not all nonresponding patients showed increased T_{reg} cell activity after treatment, indicating that other resistance mechanisms are in play and that careful selection of eligible patients is essential.

Although we were able to show activation of T_{reg} cells upon α PD-L1 treatment in mouse models of primary and acquired resistance to therapy, we did not selectively ablate PD-1 on T_{reg} cells to determine a direct causal relation of this inhibitory molecule with therapy resistance. Furthermore, the responses of T_{reg} in patients with cancer under treatment were measured retrospectively and would ideally be taken from cancer lesions instead of peripheral blood.

In summary, our findings implicate α PD-1/PD-L1-mediated activation of T_{reg} cells as an important mediator of therapy resistance. These data offer avenues for further research into the underlying mechanisms, identification of biomarkers, and treatment-induced T_{reg} cell-specific targets that could reverse α PD-1/PD-L1 resistance.

MATERIALS AND METHODS

Study design

The objective of this study was to investigate the effect of ICB using α PD-1/PD-L1 on T_{reg} cells and the association with treatment resistance. To investigate this, we used various mouse solid tumor models treated with ICB alone or in combination with T_{reg} -depleting agents α CD25 and DT in the case of DERE mice. Impact on tumor outgrowth was measured together with in vitro suppression assays, flow cytometry profiling of TME, and RNA sequencing. Patient-derived peripheral blood mononuclear cells (PBMCs) on ICB treatment were analyzed by flow cytometry, and publicly available scRNA-seq data were reanalyzed from site-matched tumor biopsies for clinical relevance. The sample size and number of biological replicates are indicated in each of the figure legends. No data were excluded from the study. In all in vivo experiments shown in the study, animals were randomized and assigned to experimental groups on the basis of sex and age. Tumor measurements were performed by a researcher blinded to each animal's treatment group. Sampling replicates are indicated in figure legends. Data collection in all mouse experiments was performed until the humane or experimental end point was reached, predetermined and approved by the national central committee of animal experiments (CCD). Data are reported according to Animal Research: Reporting of In Vivo Experiments (ARRIVE) guidelines.

Mouse models

In general, female 8- to 12-week-old C57BL/6 mice were purchased from Envigo. For the RNA sequencing experiment and the in vitro suppression assay, 10- to 12-week-old female and male FoxP3^{RFP} reporter mice were used that were obtained by in-house breeding of GATIR mice (*Gata3* knock-in reporter mice) (48) and FoxP3^{RFP} mice (49). Female and male DERE mice were purchased from the Jackson Laboratory (catalog no. 032050), bred in-house (IRC VIB, Ghent, Belgium), and used for experiments at 7 to 14 weeks of age. For the bone marrow chimera experiments, donor female and male 8-week-old PD-1^{KO} mice were purchased from the Jackson Laboratory (catalog no. 028276), bred in-house [Center for Inflammation Research (IRC) of the Flemish Institute of Biotechnology (VIB), Ghent, Belgium], and used in experiments at 14 weeks of age. In experiments where both female and male mice were used, the experimental treatment groups were sex-balanced. For the mixed chimera experiments, bone marrow from donors was sex-matched with the recipients. All mice were housed under specific pathogen-free conditions in individually ventilated cages at the animal care facility of the Erasmus MC, Rotterdam, Netherlands or at the animal facility at the IRC, Ghent University, Belgium. All mouse experiments were controlled by the animal welfare committee (IvD) of the Erasmus MC and approved by the CCD under the permit number AVD101002017867. Experiments performed at the IRC, Belgium were approved under national license LA1400019.

Mouse tumor cell lines

The OVA-transfected AE17 tumor cell line was provided by D. J. Nelson (Curtin University, Perth, Australia). The AC29 mesothelioma cell line was derived from tumors induced by crocidolite asbestos into CBA/J mice and was provided by B. W. S. Robinson (Queen Elizabeth II Medical Centre, Nedlands, Australia). The AE17-OVA and AC29 cell lines were cultured in RPMI-1640 medium containing Hepes (25 mmol/liter), Glutamax, gentamicin (50 mg/ml; all obtained from Gibco), geneticin (50 mg/ml; Gibco), and either 5% fetal bovine serum (FBS) (Capricorn Scientific) for AC29 tumor cells or 10% FBS for AE17-OVA tumor cells in a humidified atmosphere and at 5% CO₂ air. The MC38 and B16F10 tumor cell lines were cultured in IMDM medium (Gibco) containing L-glutamine, Hepes (25 mmol/liter), gentamicin (50 mg/ml), and 8% FBS. Authentication of the cell lines was performed by short tandem microsatellite repeat analysis or by antigen-specific T cell recognition.

SCLC, NSCLC, and mesothelioma patient cohorts

Patients with advanced malignant pleural mesothelioma, stage IV SCLC, and stage IV NSCLC in this study were enrolled in the MULTOMAB study (Netherlands Trial Registry: NTR7015; local ethics board study number MEC16–011). The study was approved by the institutional review board of the Netherlands Cancer Institute and in accordance with the Declaration of Helsinki. All patients provided written informed consent before enrollment. In the case of NSCLC, patients with adenocarcinoma harboring an actionable driver mutation (EGFR, no NTRK, ROS, RET, MET or BRAF were present in this study) were excluded because these respond differently to α PD-1 therapy (50, 51). Mutations in the KRAS oncogene were permitted. In summary, 21 patients with stage IV NSCLC and 15 patients with mesothelioma were treated with either nivolumab (240-mg flat dose every 2 weeks) or

pembrolizumab (200 mg every 2 weeks). Response to PD-(L)1 inhibitors was evaluated according to Response Evaluation Criteria in Solid Tumors (RECIST) criteria (version 1.1), and modified RECIST-criteria were used for pleural malignant mesothelioma (52). All patients received at least one CT scan every 6 weeks in total to assess true disease progression and pseudoprogression followed by response or ongoing response. For NSCLC, responders were defined as having a radiological response (partial response according to RECIST) after 6 weeks, whereas for mesothelioma, patients with either radiological response after 6 weeks or stable disease for longer than 12 months were classified as a responder. Clinical and pathological characteristics of all patients are summarized in table S1.

In vivo tumor inoculation

For tumor inoculation, mice were intraperitoneally injected with AE17-OVA (3.0^5) or AC29 (10^6) in 300 μ l of phosphate-buffered saline (PBS) or subcutaneously with MC38 (5.0^5) or B16F10 (1.0^5) tumor cells in 200 μ l of PBS. Subsequently, mice were randomly assigned to experimental groups. Mice with established intraperitoneal tumors were euthanized at indicated time points for immune cell profiling or when profoundly ill according to the body condition score for therapy efficacy experiments. For subcutaneous tumors, mice were euthanized at indicated time points for immune cell profiling or when the tumor reached a volume of 1500 mm³ for therapy efficacy experiments.

In vivo treatments

α PD-L1 treatment

Mice with established mesothelioma (AE17-OVA) were treated with either 200 μ g of isotype (clone 2A3, BioXCell) or 200 μ g of α PD-L1 (clone MIH5) in 300 μ l of PBS intraperitoneally (i.p.) at indicated time points. For mice with established subcutaneous MC38 tumors (colon carcinoma-derived), mice were treated with isotype (clone MPC-11, BioXCell) or 200 μ g of α PD-L1 (clone 10F.9G2, BioXCell) in 100 μ l of PBS intraperitoneally (i.p.) at days 5, 8, and 11.

DT treatment

T_{reg} cells were depleted in DERE mice using intraperitoneal injections of 1 μ g of DT (Enzo Life Sciences; BML-G135-0001) at days 8, 9, and 12.

α CD25 treatment

T_{reg} cells were depleted using intraperitoneal injections of 200 μ g of α CD25-mIgG2a PC-61.5.3 [AE17-OVA: Absolute Antibody; MC38: isotype-switched PC-61 hybridoma by CRISPR/HDR engineering (25)] at days 7 and 9 for the AE17-OVA model and at days 5 and 7 for MC38 model. As a control, mice were treated with isotype [AE17-OVA: anti-hapten 4-hydroxy-3-nitrophenyl acetyl clone B1-8 (Absolute Antibody); MC38: clone C1.18.4 (BioXCell)].

Preparation of single-cell suspensions from mouse tissues

Single-cell suspensions were generated from isolated blood, spleen, non-TDLN, TDLN, bone marrow, and tumor tissue of mice from each group as previously reported (53). Briefly, blood was collected in EDTA tubes (Microvette CB300, Sarstedt), after which the volume was determined. Subsequently, collected blood was lysed by erythrocyte lysis using osmotic lysis buffer (8.3% NH₄Cl, 1% KHCO₃, and 0.04% Na₂EDTA in Milli-Q). Single-cell suspensions of non-TDLNs, TDLNs, bone marrow, and spleens were generated by mechanically dispersing the lymph nodes through a 100- μ m

nylon mesh cell strainer (BD Biosciences) followed by osmotic lysis of erythrocytes in the case of spleens. Tumors were collected, weighed in a microbalance, and dissociated using a validated tumor dissociation system (Miltenyi Biotec) according to protocol. After dissociation, cell suspensions were filtered through a 100- μ m nylon mesh cell strainer.

In vitro suppression assay

For in vitro suppression assays with tumor-derived T_{reg} cells, AE17-OVA-bearing mice were treated with isotype or α PD-L1 at days 10 and 13. At day 17, mice were euthanized, and CD4⁺RFP⁺ cells were sorted from AE17-OVA tumors. Splenic CD4⁺CD25⁺RFP⁺ cells were sorted at day 13, 3 days after treatment with either isotype or α PD-L1 at day 10. Splenic naive CD8⁺ T cells from wild-type mice (responder cells, T_{resp}) were isolated using negative magnetic labeling (Miltenyi) and were labeled with CellTrace Far Red Cell Proliferation dye (Thermo Fisher Scientific). For APCs, wild-type splenocytes were T cell-depleted (CD90.2 microbeads; Miltenyi Biotec) and treated with mitomycin-c (Sigma-Aldrich) to prevent the proliferation of APCs, which could influence the readout of the assay. Responder cells (1×10^4), APCs (16.7×10^3), and titrated numbers of T_{reg} cells were activated with anti-CD3 (0.5 μ g/ml; BD Biosciences) in a 96-well round bottom plate with 200 μ l of IMDM supplemented with gentamycin (50 mg/ml), 50 mM β -ME, and 10% fetal calf serum (FCS) for 3 days. Suppression was calculated as previously described (54). Briefly, cells were acquired by BD Symphony, and the division index of responder cells was analyzed using FlowJo on the basis of the division of CellTrace FarRed. Suppression was then calculated with the formula % Suppression = $(1 - \text{DIT}_{\text{reg}} \text{ cells/DICtrl}) \times 100\%$ (DIT_{reg} cells stands for the division index of responder cells with T_{reg} cells, and DICtrl stands for the division index of responder cells activated without T_{reg} cells).

RNA sequencing

RNA was isolated from sorted tumor-derived T_{reg} cells. Tumor-derived T_{reg} cells were isolated from AE17-OVA tumor-bearing FoxP3^{RFP} mice treated with isotype or with α PD-L1 3 days after treatment at day 10. For the isolation of T_{reg} cells, tumor samples were stained with antibodies listed in table S3 and subsequently sorted using a FACSAria III sorter with a purity $\geq 98\%$ (number of sorted PD-1^{+/-} T_{reg} cells ranged between 900 and 7000 cells). RNA was isolated using the RNeasy Micro kit (Qiagen) according to the manufacturer's instruction. Library preparation was based on the Smart-seq2 protocol (55). Samples were sequenced in accordance with the Illumina TruSeq Rapid v2 protocol on an Illumina HiSeq 2500 to obtain 50-bp single-end reads. Reads were aligned to the mm10 (GRCm38) mouse genome using HISAT2 (56). To identify DEGs, DESeq2 was used as implemented in HOMER (57, 58), and read alignment was performed to the murine genome mm10 (GRCm38). Sample scaling and statistical analysis were performed using the R package DESeq2. DEGs were determined by >1.0 absolute log₂ fold change and an adjusted *P* value < 0.05 . Standard reads per kilobase per million (RPKM) values were used as an absolute measure of gene expression. Genes with an RPKM < 1 in 50% of replicates in one condition were excluded. To assess sample quality, principal components analysis was conducted on using log-transformed RPKM values using the prcomp function from the ggfortify (0.4.11) package in R (executed from R Studio v1.1.383). K-means clustering was performed using Past3 software.

Heatmaps were produced using the web-based tool Morpheus (<https://software.broadinstitute.org/morpheus>). Pathway enrichment was performed using the web-based tool Metascape (59).

Bone marrow chimeras

CD45.1.2 host mice were administered a single total body gamma radiation of 8 Gy. Donor CD45.1 wild-type mice and CD45.2 PD-1^{KO} mice were euthanized by cervical dislocation, and femurs were harvested and collected in RPMI. Bone marrow cells were isolated in a sterile environment by flushing the femur with a 20-G needle using PBS and 2% FBS. Red blood cells were lysed using RBC lysis buffer (eBioscience; 00-4333-57) and washed using PBS. Harvested cells were filtered through a 40- μ m cell filter and counted. Donor mixes were prepared by mixing CD45.1 and CD45.2 cells in a 1:1 ratio in sterile PBS. From both CD45.1 and CD45.2 bone marrow cells, 3.0×10^6 were transplanted via the tail vein in a total volume of 100 μ l. After 8 weeks of reconstitution, transplanted hosts were bled via the tail vein to confirm chimerism and assess circulating lymphocyte populations. On the same day, host mice were intraperitoneally injected with AE17-OVA tumor cells. Host mice were treated with either isotype or α PD-L1 10 days after tumor inoculation and euthanized at day 13, and bone marrow, spleen, blood, non-TDLNs, TDLNs, and tumors were harvested for characterization of T_{reg} cells.

Reanalysis of scRNA-seq data

scRNA-seq data analysis

Publicly available scRNA-seq data were analyzed using the Seurat (4.0.0) package. Predefined T_{reg} cell clusters were isolated and processed for downstream analysis. We excluded cells in which fewer than 500 genes were detected and those that had a mitochondrial DNA content greater than 10%. Next, we used a zero-inflated negative binomial model implemented by the DESingle package (v1.10.0) in R to identify DEGs (60). Genes with an absolute log₂ fold change > 0.5 and an adjusted *P* value [false discovery rate (FDR)] < 0.05 were deemed significantly differentially expressed.

scRNA-seq data visualization

Violin plots were generated using log-normalized counts with a scaling factor of 10,000 using the Seurat package. Unweighted pathway enrichment analysis was performed using the web-based tool Metascape (59). Weighted pathway enrichment analysis was performed via GSEA using the ClusterProfiler (v3.18.1) package in R. Genes with an absolute log₂ fold change > 0.5 were included in the analysis. Genesets included in "biological process" were selected from MsigDB (<http://software.broadinstitute.org/gsea/msigdb>). GSEA was run with a minimum geneset size of 10 and nPermSimple = 100,000. GSEA plots were superimposed in Adobe Illustrator and plotted with the normalized enrichment score (NES) and *P* value. Heatmaps were created using the R package Pheatmap (v1.0.12) using the normalized mean expression per cell as calculated by DESingle.

Patient-derived peripheral blood processing

Peripheral blood was collected at day 1 of cycle 1 (before start of therapy; baseline) and at day 1 of cycle 2. About 50 ml of blood was collected in EDTA tubes, and PBMCs were isolated by density gradient centrifugation using Ficoll-hypaque (GE Healthcare). Cells were cryopreserved in 10% dimethylsulfoxide (Sigma-Aldrich), 40% FCS, and RPMI for later reconstitution and analysis.

Flow cytometry

Murine samples

For cell surface staining, single cells were stained with antibodies for 30 min at 4°C. After this incubation period, cells were washed with fluorescence-activated cell sorting (FACS) buffer (0.05% NaN₃ and 2% bovine serum albumin in PBS), followed by a PBS wash, and stained for viability using fixable LIVE/DEAD aqua cell stain (Thermo Fisher Scientific, 1:200) at 4°C for 15 min. After two washing steps with PBS and FACS buffer, cells were fixated and permeabilized with Foxp3 / Transcription Factor Staining Buffer Set (Thermo Fisher Scientific) to stain nuclear factors. Intranuclear antibodies were incubated for 60 min at 4°C. A fixed number of counting beads (Polysciences Inc.) was added to the samples derived from blood before acquisition of the data to determine the absolute number of cells. Data were acquired using a FACSymphony flow cytometer equipped with four lasers and FACSDiva software (v.8.0.2) after compensation with UltraComp Compensation beads (Thermo Fisher Scientific). Acquired data were analyzed using a licensed version of Flowjo (v.10.4.2). A list of antibodies used can be found in table S3.

Human samples

To assess PD-1 expression in peripheral blood isolated from ICB-treated patients by flow cytometry, cells were preincubated with either nivolumab or pembrolizumab (depending on in vivo treatment) for 20 min at 4°C (61). Subsequently, cells were stained with a biotinylated α IgG4 antibody (Sigma-Aldrich, 1:100) that specifically binds to nivolumab and pembrolizumab. Last, cells were incubated with streptavidin that specifically binds to the α IgG4 antibody. Extracellular staining with other antibodies of interest, fixation and permeabilization, and subsequent intracellular staining was according to the protocol for murine samples. Data were acquired using a FACSymphony flow cytometer equipped with four lasers and FACSDiva software (v.8.0.2) after compensation with UltraComp Compensation beads (Thermo Fisher Scientific). Acquired data were analyzed using a licensed version of Flowjo (v.10.4.2).

Statistical analysis

Data are expressed as means with the SEM. Comparisons between two groups with independent samples were performed using unpaired *t* test, whereas the paired *t* test was used to compare paired samples (see figure legends). In the case of multiple comparisons, one-way or two-way analysis of variance (ANOVA) was used with Šidák's post-test or Tukey's post-test, respectively. Survival data were plotted as Kaplan-Meier survival curves using the log-rank test to determine statistical significance. A *P* value of 0.05 and below was considered significant (*), and *P* < 0.01(**) and *P* < 0.001 (***) were considered highly significant. Statistical approaches were verified per figure. All DEG analyses were Benjamini-Hochberg-corrected for FDR (FDR < 0.05). Data were analyzed using GraphPad Prism software (Graphpad, V5.01 and V8.0).

Supplementary Materials

This PDF file includes:

Figs. S1 to S12
Tables S1 to S3

Other Supplementary Material for this manuscript includes the following:

Data file S1

MDAR Reproducibility Checklist

[View/request a protocol for this paper from Bio-protocol.](#)**REFERENCES AND NOTES**

- M. Yarchoan, A. Hopkins, E. M. Jaffee, Tumor mutational burden and response rate to PD-1 inhibition. *N. Engl. J. Med.* **377**, 2500–2501 (2017).
- F. Dammeyer, S. P. Lau, C. H. J. van Eijck, S. H. van der Burg, J. G. J. V. Aerts, Rationally combining immunotherapies to improve efficacy of immune checkpoint blockade in solid tumors. *Cytokine Growth Factor Rev.* **36**, 5–15 (2017).
- A. Ribas, J. D. Wolchok, Cancer immunotherapy using checkpoint blockade. *Science* **359**, 1350–1355 (2018).
- M. J. van Elsas, T. van Hall, S. H. van der Burg, Future challenges in cancer resistance to immunotherapy. *Cancers* **12**, 935 (2020).
- Y. Togashi, K. Shitara, H. Nishikawa, Regulatory T cells in cancer immunosuppression - implications for anticancer therapy. *Nat. Rev. Clin. Oncol.* **16**, 356–371 (2019).
- B. Shang, Y. Liu, S.-j. Jiang, Y. Liu, Prognostic value of tumor-infiltrating FoxP3⁺ regulatory T cells in cancers: A systematic review and meta-analysis. *Sci. Rep.* **5**, 15179 (2015).
- P. Sharma, S. Hu-Lieskovan, J. A. Wargo, A. Ribas, Primary, adaptive, and acquired resistance to cancer immunotherapy. *Cell* **168**, 707–723 (2017).
- F. Arce Vargas, A. J. S. Furness, I. Solomon, K. Joshi, L. Mekkaoui, M. H. Lesko, E. Miranda Rota, R. Dahan, A. Georgiou, A. Sledzinska, A. Ben Aissa, D. Franz, M. Werner Sunderland, Y. N. S. Wong, J. Y. Henry, T. O'Brien, D. Nicol, B. Challacombe, S. A. Beers, T. C. Melanoma, T. C. Renal, T. C. Lung, S. Turajlic, M. Gore, J. Larkin, C. Swanton, K. A. Chester, M. Pule, J. V. Ravetch, T. Marafioti, K. S. Peggs, S. A. Quezada, P. Crosbie, Fc-optimized anti-CD25 depletes tumor-infiltrating regulatory T cells and synergizes with PD-1 blockade to eradicate established tumors. *Immunity* **46**, 577–586 (2017).
- P. Penalzoza-MacMaster, A. O. Kamphorst, A. Wieland, K. Araki, S. S. Iyer, E. E. West, L. O'Mara, S. Yang, B. T. Konieczny, A. H. Sharpe, G. J. Freeman, A. Y. Rudensky, R. Ahmed, Interplay between regulatory T cells and PD-1 in modulating T cell exhaustion and viral control during chronic LCMV infection. *J. Exp. Med.* **211**, 1905–1918 (2014).
- J. Liu, S. J. Blake, H. Harjunpaa, K. A. Fairfax, M. C. Yong, S. Allen, H. E. Kohrt, K. Takeda, M. J. Smyth, M. W. L. Teng, Assessing immune-related adverse events of efficacious combination immunotherapies in preclinical models of cancer. *Cancer Res.* **76**, 5288–5301 (2016).
- D. A. Vignali, L. W. Collison, C. J. Workman, How regulatory T cells work. *Nat. Rev. Immunol.* **8**, 523–532 (2008).
- K. Wing, Y. Onishi, P. Prieto-Martin, T. Yamaguchi, M. Miyara, Z. Fehervari, T. Nomura, S. Sakaguchi, CTLA-4 control over Foxp3⁺ regulatory T cell function. *Science* **322**, 271–275 (2008).
- T. Okazaki, S. Chikuma, Y. Iwai, S. Fagarasan, T. Honjo, A rheostat for immune responses: The unique properties of PD-1 and their advantages for clinical application. *Nat. Immunol.* **14**, 1212–1218 (2013).
- D. B. Flies, B. J. Sandler, M. Sznol, L. Chen, Blockade of the B7-H1/PD-1 pathway for cancer immunotherapy. *Yale J. Biol. Med.* **84**, 409–421 (2011).
- J. L. Riley, PD-1 signaling in primary T cells. *Immunol. Rev.* **229**, 114–125 (2009).
- S. Kumagai, Y. Togashi, T. Kamada, E. Sugiyama, H. Nishinakamura, Y. Takeuchi, K. Vitaly, K. Itahashi, Y. Maeda, S. Matsui, T. Shibahara, Y. Yamashita, T. Irie, A. Tsuge, S. Fukuoka, A. Kawazoe, H. Udagawa, K. Kirita, K. Aokage, G. Ishii, T. Kuwata, K. Nakama, M. Kawazu, T. Ueno, N. Yamazaki, K. Goto, M. Tsuboi, H. Mano, T. Doi, K. Shitara, H. Nishikawa, The PD-1 expression balance between effector and regulatory T cells predicts the clinical efficacy of PD-1 blockade therapies. *Nat. Immunol.* **21**, 1346–1358 (2020).
- T. Kamada, Y. Togashi, C. Tay, D. Ha, A. Sasaki, Y. Nakamura, E. Sato, S. Fukuoka, Y. Tada, A. Tanaka, H. Morikawa, A. Kawazoe, T. Kinoshita, K. Shitara, S. Sakaguchi, H. Nishikawa, PD-1⁺ regulatory T cells amplified by PD-1 blockade promote hyperprogression of cancer. *Proc. Natl. Acad. Sci. U.S.A.* **116**, 9999–10008 (2019).
- L. Strauss, M. A. A. Mahmoud, J. D. Weaver, N. M. Tijaro-Ovalle, A. Christofides, Q. Wang, R. Pal, M. Yuan, J. Asara, N. Patsoukis, V. A. Boussiotis, Targeted deletion of PD-1 in myeloid cells induces antitumor immunity. *Sci. Immunol.* **5**, eaay1863 (2020).
- I. Shalev, H. Liu, C. Kosciak, A. Bartczak, M. Javadi, K. M. Wong, A. Maknoja, W. He, M. F. Liu, J. Diao, E. Winter, J. Manuel, D. McCarthy, M. Cattral, J. Gommerman, D. A. Clark, M. J. Phillips, R. R. Gorczynski, L. Zhang, G. Downey, D. Grant, M. I. Cybulsky, G. Levy, Targeted deletion of *fgl2* leads to impaired regulatory T cell activity and development of autoimmune glomerulonephritis. *J. Immunol.* **180**, 249–260 (2008).
- A. Chruscinski, H. Sadozai, V. Rojas-Luengas, A. Bartczak, R. Khattar, N. Selznar, G. A. Levy, Role of regulatory T cells (Treg) and the Treg effector molecule fibrinogen-like protein 2 in alloimmunity and autoimmunity. *Rambam Maimonides Med. J.* **6**, e0024 (2015).
- Y. Park, H. S. Jin, J. Lopez, C. Elly, G. Kim, M. Murai, M. Kronenberg, Y. C. Liu, TSC1 regulates the balance between effector and regulatory T cells. *J. Clin. Invest.* **123**, 5165–5178 (2013).
- E. Mouly, K. Chemin, H. V. Nguyen, M. Chopin, L. Mesnard, M. Leite-de-Moraes, O. Burlen-defranoux, A. Bandeira, J. C. Bories, The Ets-1 transcription factor controls the development and function of natural regulatory T cells. *J. Exp. Med.* **207**, 2113–2125 (2010).
- J. K. Polansky, L. Schreiber, C. Thelemann, L. Ludwig, M. Kruger, R. Baumgrass, S. Cording, S. Floess, A. Hamann, J. Huehn, Methylation matters: Binding of Ets-1 to the demethylated Foxp3 gene contributes to the stabilization of Foxp3 expression in regulatory T cells. *J. Mol. Med. (Berl)* **88**, 1029–1040 (2010).
- T. Maj, W. Wang, J. Crespo, H. Zhang, W. Wang, S. Wei, L. Zhao, L. Vatan, I. Shao, W. Szeliga, C. Lyssiotis, J. R. Liu, I. Kryczek, W. Zou, Oxidative stress controls regulatory T cell apoptosis and suppressor activity and PD-L1-blockade resistance in tumor. *Nat. Immunol.* **18**, 1332–1341 (2017).
- M. J. van Elsas, J. M. S. van der Schoot, A. Bartels, K. Steuten, D. van Dalen, Z. Wijffes, C. G. Figdor, T. van Hall, S. H. van der Burg, M. Verdoes, F. A. Scheeren, Regulatory T cell depletion using a CRISPR Fc-optimized CD25 antibody. *Int. J. Mol. Sci.* **23**, 8707 (2022).
- K. E. Yost, A. T. Satpathy, D. K. Wells, Y. Qi, C. Wang, R. Kageyama, K. L. McNamara, J. M. Granja, K. Y. Sarin, R. A. Brown, R. K. Gupta, C. Curtis, S. L. Bucktrout, M. M. Davis, A. L. S. Chang, H. Y. Chang, Clonal replacement of tumor-specific T cells following PD-1 blockade. *Nat. Med.* **25**, 1251–1259 (2019).
- B. Liu, X. Hu, K. Feng, R. Gao, Z. Xue, S. Zhang, Y. Zhang, E. Corse, Y. Hu, W. Han, Z. Zhang, Temporal single-cell tracing reveals clonal revival and expansion of precursor exhausted T cells during anti-PD-1 therapy in lung cancer. *Nat. Cancer* **3**, 108–121 (2022).
- L. Horn, A. S. Mansfield, A. Szczesna, L. Havel, M. Krzakowski, M. J. Hochmair, F. Huemer, G. Losonczy, M. L. Johnson, M. Nishio, M. Reck, T. Mok, S. Lam, D. S. Shames, J. Liu, B. Ding, A. Lopez-Chavez, F. Kabbinar, W. Lin, A. Sandler, S. V. Liu, I. M. S. Group, First-line Atezolizumab plus chemotherapy in extensive-stage small-cell lung cancer. *N. Engl. J. Med.* **379**, 2220–2229 (2018).
- S. J. Antonia, J. A. Lopez-Martin, J. Bendell, P. A. Ott, M. Taylor, J. P. Eder, D. Jager, M. C. Pietanza, D. T. Le, F. de Braud, M. A. Morse, P. A. Ascierto, L. Horn, A. Amin, R. N. Pillai, J. Evans, I. Chau, P. Bono, A. Atmaca, P. Sharma, C. T. Harbison, C. S. Lin, O. Christensen, E. Calvo, Nivolumab alone and nivolumab plus ipilimumab in recurrent small-cell lung cancer (CheckMate 032): A multicentre, open-label, phase 1/2 trial. *Lancet Oncol.* **17**, 883–895 (2016).
- M. Nishino, N. H. Ramaiya, H. Hatabu, F. S. Hodi, Monitoring immune-checkpoint blockade: Response evaluation and biomarker development. *Nat. Rev. Clin. Oncol.* **14**, 655–668 (2017).
- T. Asano, Y. Meguri, T. Yoshioka, Y. Kishi, M. Iwamoto, M. Nakamura, Y. Sando, H. Yagita, J. Koreth, H. T. Kim, E. P. Alyea, P. Armand, C. S. Cutler, V. T. Ho, J. H. Antin, R. J. Soiffer, Y. Maeda, M. Tanimoto, J. Ritz, K. I. Matsuoka, PD-1 modulates regulatory T-cell homeostasis during low-dose interleukin-2 therapy. *Blood* **129**, 2186–2197 (2017).
- S. C. Vick, O. V. Kolupaev, C. M. Perou, J. S. Serody, Anti-PD-1 checkpoint therapy can promote the function and survival of regulatory T cells. *J. Immunol.* **207**, 2598–2607 (2021).
- B. Zhang, S. Chikuma, S. Hori, S. Fagarasan, T. Honjo, Nonoverlapping roles of PD-1 and FoxP3 in maintaining immune tolerance in a novel autoimmune pancreatitis mouse model. *Proc. Natl. Acad. Sci. U.S.A.* **113**, 8490–8495 (2016).
- C. L. Tan, J. R. Kuchroo, P. T. Sage, D. Liang, L. M. Francisco, J. Buck, Y. R. Thaker, Q. Zhang, S. L. McArde, V. R. Juneja, S. J. Lee, S. B. Lovitch, C. Lian, G. F. Murphy, B. R. Blazar, D. A. A. Vignali, G. J. Freeman, A. H. Sharpe, PD-1 restraint of regulatory T cell suppressive activity is critical for immune tolerance. *J. Exp. Med.* **218**, e20182232 (2021).
- J. A. Perry, L. Shallberg, J. T. Clark, J. A. Gullicksrud, J. H. DeLong, B. B. Douglas, A. P. Hart, Z. Lanzar, K. O'Dea, C. Konradt, J. Park, J. R. Kuchroo, D. Grubaugh, A. G. Zaretsky, I. E. Brodsky, R. W. Malefyt, D. A. Christian, A. H. Sharpe, C. A. Hunter, PD-L1-PD-1 interactions limit effector regulatory T cell populations at homeostasis and during infection. *Nat. Immunol.* **23**, 743–756 (2022).
- A. E. Overacre-Delgoffe, M. Chikina, R. E. Dadey, H. Yano, E. A. Brunazzi, G. Shayan, W. Horne, J. M. Moskovitz, J. K. Kolls, C. Sander, Y. Shuai, D. P. Normolle, J. M. Kirkwood, R. L. Ferris, G. M. Delgoffe, T. C. Bruno, C. J. Workman, D. A. A. Vignali, Interferon- γ drives Treg fragility to promote anti-tumor immunity. *Cell* **169**, 1130–1141.e11 (2017).
- H. Wang, F. Franco, Y. C. Tsui, X. Xie, M. P. Trefny, R. Zappasodi, S. R. Mohmood, J. Fernandez-Garcia, C. H. Tsai, I. Schulze, F. Picard, E. Meylan, R. Silverstein, I. Goldberg, S. M. Fendt, J. D. Wolchok, T. Merghoub, C. Jandus, A. Zippelius, P. C. Ho, CD36-mediated metabolic adaptation supports regulatory T cell survival and function in tumors. *Nat. Immunol.* **21**, 298–308 (2020).
- M. J. Watson, P. D. A. Vignali, S. J. Mullett, A. E. Overacre-Delgoffe, R. M. Peralta, S. Grebinoski, A. V. Menk, N. L. Rittenhouse, K. DePeaux, R. D. Whetstone, D. A. A. Vignali,

- T. W. Hand, A. C. Poholek, B. M. Morrison, J. D. Rothstein, S. G. Wendell, G. M. Delgoffe, Metabolic support of tumour-infiltrating regulatory T cells by lactic acid. *Nature* **591**, 645–651 (2021).
39. S. A. Lim, J. Wei, T. M. Nguyen, H. Shi, W. Su, G. Palacios, Y. Dhungana, N. M. Chapman, L. Long, J. Saravia, P. Vogel, H. Chi, Lipid signalling enforces functional specialization of T_{reg} cells in tumours. *Nature* **591**, 306–311 (2021).
40. H. Li, A. M. van der Leun, I. Yofe, Y. Lubling, D. Gelbard-Solodkin, A. C. J. van Akkooi, M. van den Braber, E. A. Rozeman, J. Haanen, C. U. Blank, H. M. Horlings, E. David, Y. Baran, A. Bercovich, A. Lifshitz, T. N. Schumacher, A. Tanay, I. Amit, Dysfunctional CD8 T cells form a proliferative, dynamically regulated compartment within human melanoma. *Cell* **176**, 775–789.e18 (2019).
41. M. Sade-Feldman, K. Yizhak, S. L. Bjorgaard, J. P. Ray, C. G. de Boer, R. W. Jenkins, D. J. Lieb, J. H. Chen, D. T. Frederick, M. Barzily-Rokni, S. S. Freeman, A. Reuben, P. J. Hoover, A. C. Villani, E. Ivanova, A. Portell, P. H. Lizotte, A. R. Aref, J. P. Eliane, M. R. Hammond, H. Vitzthum, S. M. Blackmon, B. Li, V. Gopalakrishnan, S. M. Reddy, Z. A. Cooper, C. P. Paweletz, D. A. Barbie, A. Stemmer-Rachamimov, K. T. Flaherty, J. A. Wargo, G. M. Boland, R. J. Sullivan, G. Getz, N. Hacohen, Defining T cell states associated with response to checkpoint immunotherapy in melanoma. *Cell* **175**, 998–1013.e20 (2018).
42. F. Dammeyer, M. van Gulijk, E. E. Mulder, M. Lukkes, L. Klaase, T. van den Bosch, M. van Nimwegen, S. P. Lau, K. Latupeirissa, S. Schetters, Y. van Kooyk, L. Boon, A. Moyaart, Y. M. Mueller, P. D. Katsikis, A. M. Eggermont, H. Vroman, R. Stadhouders, R. W. Hendriks, J. V. Thusen, D. J. Grunhagen, C. Verhoef, T. van Hall, J. G. Aerts, The PD-1/PD-L1-checkpoint restrains T cell immunity in tumor-draining lymph nodes. *Cancer Cell* **38**, 685–700.e8 (2020).
43. N. G. Nunez, J. Tosello Boari, R. N. Ramos, W. Richer, N. Cagnard, C. D. Anderfuhren, L. L. Niborski, J. Bigot, D. Meseure, P. De La Rochere, M. Milder, S. Viel, D. Loirat, L. Perol, A. Vincent-Salomon, X. Sastre-Garau, B. Burkhard, C. Sedlik, O. Lantz, S. Amigorena, E. Piaggio, Tumor invasion in draining lymph nodes is associated with Treg accumulation in breast cancer patients. *Nat. Commun.* **11**, 3272 (2020).
44. I. Solomon, M. Amann, A. Goubier, F. A. Vargas, D. Zervas, C. Qing, J. Y. Henry, E. Ghorani, A. U. Akarca, T. Marafioti, A. Sledzinska, M. W. Sunderland, D. F. Demane, J. R. Clancy, A. Georgiou, J. Salimu, P. Merchiers, M. A. Brown, R. Flury, J. Eckmann, C. Murgia, J. Sam, B. Jacobsen, E. Marrer-Berger, C. Boetsch, S. Belli, L. Leibrock, J. Benz, H. Koll, R. Suttmüller, K. S. Peggs, S. A. Quezada, CD25-T_{reg}-depleting antibodies preserving IL-2 signaling on effector T cells enhance effector activation and antitumor immunity. *Nat Cancer* **1**, 1153–1166 (2020).
45. M. J. A. Schoonderwoerd, M. F. M. Koops, R. A. Angela, B. Koolmoes, M. Toitou, M. Paauwe, M. C. Barnhoorn, Y. Liu, C. F. M. Sier, J. C. H. Hardwick, A. B. Nixon, C. P. Theuer, M. F. Fransen, L. J. A. C. Hawinkels, Targeting endoglin-expressing regulatory T cells in the tumor microenvironment enhances the effect of pd1 checkpoint inhibitor immunotherapy. *Clin. Cancer Res.* **26**, 3831–3842 (2020).
46. S. Kumagai, S. Koyama, K. Itahashi, T. Tanegashima, Y. T. Lin, Y. Togashi, T. Kamada, T. Irie, G. Okumura, H. Kono, D. Ito, R. Fujii, S. Watanabe, A. Sai, S. Fukuoka, E. Sugiyama, G. Watanabe, T. Owari, H. Nishinakamura, D. Sugiyama, Y. Maeda, A. Kawazoe, H. Yukami, K. Chida, Y. Ohara, T. Yoshida, Y. Shinno, Y. Takeyasu, M. Shirasawa, K. Nakama, K. Aokage, J. Suzuki, G. Ishii, T. Kuwata, N. Sakamoto, M. Kawazu, T. Ueno, T. Mori, N. Yamazaki, M. Tsuboi, Y. Yatabe, T. Kinoshita, T. Doi, K. Shitara, H. Mano, H. Nishikawa, Lactic acid promotes PD-1 expression in regulatory T cells in highly glycolytic tumor microenvironments. *Cancer Cell* **40**, 201–218.e9 (2022).
47. K. Itahashi, T. Irie, J. Yuda, S. Kumagai, T. Tanegashima, Y. T. Lin, S. Watanabe, Y. Goto, J. Suzuki, K. Aokage, M. Tsuboi, Y. Minami, G. Ishii, Y. Ohe, W. Ise, T. Kurosaki, Y. Suzuki, S. Koyama, H. Nishikawa, BATF epigenetically and transcriptionally controls the activation program of regulatory T cells in human tumors. *Sci. Immunol.* **7**, eabk0957 (2022).
48. T. N. Rao, S. Kumar, A. J. Pulikkottil, F. Oliveri, R. W. Hendriks, F. Beckel, H. J. Fehling, Novel, non-gene-destructive knock-in reporter mice refute the concept of monoallelic *Gata3* expression. *J. Immunol.* **204**, 2600–2611 (2020).
49. Y. Y. Wan, R. A. Flavell, Identifying Foxp3-expressing suppressor T cells with a bicistronic reporter. *Proc. Natl. Acad. Sci. U.S.A.* **102**, 5126–5131 (2005).
50. J. Mazieres, A. Drilon, A. Lusque, L. Mhanna, A. B. Cortot, L. Mezquita, A. A. Thai, C. Mascoux, S. Couraud, R. Veillon, M. Van den Heuvel, J. Neal, N. Peled, M. Früh, T. L. Ng, V. Gounant, S. Popat, J. Diebold, J. Sabari, V. W. Zhu, S. I. Rothschild, P. Bironzo, A. Martinez-Marti, A. Curioni-Fontecedro, R. Rosell, M. Lattuca-Truc, M. Wiesweg, B. Besse, B. Solomon, F. Barlesi, R. D. Schouten, H. Wakelee, D. R. Camidge, G. Zalcman, S. Novello, S. I. Ou, J. Milia, O. Gautschi, Immune checkpoint inhibitors for patients with advanced lung cancer and oncogenic driver alterations: Results from the IMMUNOTARGET registry. *Ann. Oncol.* **30**, 1321–1328 (2019).
51. J. F. Gainor, A. T. Shaw, L. V. Sequist, X. Fu, C. G. Azzoli, Z. Piotrowska, T. G. Huynh, L. Zhao, L. Fulton, K. R. Schultz, E. Howe, A. F. Farago, R. J. Sullivan, J. R. Stone, S. Digumarthy, T. Moran, A. N. Hata, Y. Yagi, B. Y. Yeap, J. A. Engelman, M. Mino-Kenudson, *EGFR* mutations and *ALK* rearrangements are associated with low response rates to PD-1 pathway blockade in non-small cell lung cancer: A retrospective analysis. *Clin. Cancer Res.* **22**, 4585–4593 (2016).
52. A. S. Tsao, L. Garland, M. Redman, K. Kernstine, D. Gandara, E. M. Marom, A practical guide of the Southwest Oncology Group to measure malignant pleural mesothelioma tumors by RECIST and modified RECIST criteria. *J. Thorac. Oncol.* **6**, 598–601 (2011).
53. F. Dammeyer, L. A. Lievense, M. E. Kaijen-Lambers, M. van Nimwegen, K. Bezemer, J. P. Hegmans, T. van Hall, R. W. Hendriks, J. G. Aerts, Depletion of tumor-associated macrophages with a CSF-1R kinase inhibitor enhances antitumor immunity and survival induced by DC immunotherapy. *Cancer Immunol. Res.* **5**, 535–546 (2017).
54. A. N. McMurchy, M. K. Levings, Suppression assays with human T regulatory cells: A technical guide. *Eur. J. Immunol.* **42**, 27–34 (2012).
55. S. Picelli, A. K. Bjorklund, O. R. Faridani, S. Sagasser, G. Winberg, R. Sandberg, Smart-seq2 for sensitive full-length transcriptome profiling in single cells. *Nat. Methods* **10**, 1096–1098 (2013).
56. D. Kim, B. Langmead, S. L. Salzberg, HISAT: A fast spliced aligner with low memory requirements. *Nat. Methods* **12**, 357–360 (2015).
57. M. I. Love, W. Huber, S. Anders, Moderated estimation of fold change and dispersion for RNA-seq data with DESeq2. *Genome Biol.* **15**, 550 (2014).
58. S. Heinz, C. Benner, N. Spann, E. Bertolino, Y. C. Lin, P. Laslo, J. X. Cheng, C. Murre, H. Singh, C. K. Glass, Simple combinations of lineage-determining transcription factors prime cis-regulatory elements required for macrophage and B cell identities. *Mol. Cell* **38**, 576–589 (2010).
59. Y. Zhou, B. Zhou, L. Pache, M. Chang, A. H. Khodabakhshi, O. Tanaseichuk, C. Benner, S. K. Chanda, Metascape provides a biologist-oriented resource for the analysis of systems-level datasets. *Nat. Commun.* **10**, 1523 (2019).
60. Z. Miao, K. Deng, X. Wang, X. Zhang, Dsingle for detecting three types of differential expression in single-cell RNA-seq data. *Bioinformatics* **34**, 3223–3224 (2018).
61. H. Zelba, J. Bochem, G. Pawelec, C. Garbe, K. Wistuba-Hamprecht, B. Weide, Accurate quantification of T-cells expressing PD-1 in patients on anti-PD-1 immunotherapy. *Cancer Immunol. Immunother.* **67**, 1845–1851 (2018).

Acknowledgments: We would like to thank R. Hendriks for helpful discussions and S. Baart for the statistical assistance. In addition, we would like to acknowledge all involved technicians from the pulmonary medicine department and the animal facility at the Erasmus Medical Center and Leiden University Medical Center for valuable contributions to this project.

Funding: M.v.G. is supported by the Mesothelioma Applied Research Foundation (MARF). S.H.v.d.B. is a recipient of the Onco Institute base fund, and R.S. is supported by an Erasmus MC Fellowship, a Dutch Lung Foundation Junior Investigator grant (4.2.19.041JO), a Daniel den Hoed Foundation grant, and a VIDJ grant (09150172010068) from the Dutch Research Council (NWO). **Author contributions:** M.v.G., F.D., T.v.H., and J.A. designed the experiments. M.v.G., M.E., L.K., M.d.B., M.v.N., and T.v.T. performed murine experiments, and M.v.G. analyzed the data. M.v.G., A.v.K., and R.S. performed the RNA sequencing analyses. L.B. provided therapeutic aPD-L1 antibody. J.v.d.S., M.V., and F.S. engineered the aCD25 antibody. M.v.G., F.D., T.v.H., and J.A. wrote the manuscript. All authors were involved in the critical review of the manuscript. All authors read and approved the manuscript. **Competing Interests:** The authors declare that they have no competing interests. **Data and materials availability:** Original RNA sequencing data have been deposited to GEO: GSE176250. All data needed to evaluate the conclusions in the paper are present in the paper or the Supplementary Materials.

Submitted 8 December 2021
Resubmitted 06 January 2023
Accepted 24 April 2023
Published 19 May 2023
10.1126/sciimmunol.abn6173